Hindawi
Adsorption Science & Technology
Volume 2022, Article ID 9056288, 20 pages
https://doi.org/10.1155/2022/9056288

Research Article

Eco-Friendly Detoxification of Congo Red Dye from Water by Citric Acid Activated Bioadsorbents Consisting of Watermelon and Water Chestnuts Peels Collected from Indigenous Resources

Muhammad Sadiq Hussain,[1] Rabia Rehman,[1] Muhammad Imran,[1] Amara Dar,[2] Mehwish Akram,[3] and Eman A. Al-Abbad[4]

[1]*Centre for Inorganic Chemistry, School of Chemistry, University of the Punjab, Quaid-e-Azam Campus, Lahore 54590, Pakistan*
[2]*Centre for Analytical Chemistry, School of Chemistry, University of the Punjab, Quaid-e-Azam Campus, Lahore 54590, Pakistan*
[3]*Institute of Geology, University of the Punjab, Quaid-e-Azam Campus, Lahore 54590, Pakistan*
[4]*Department of Chemistry, College of Science, Imam Abdulrahman Bin Faisal University, P.O.Box 1982, Dammam 31441, Saudi Arabia*

Correspondence should be addressed to Rabia Rehman; grinorganic@yahoo.com

Received 9 May 2022; Revised 6 July 2022; Accepted 20 July 2022; Published 8 August 2022

Academic Editor: Stefano Salvestrini

The native peels of two cheap, locally available adsorbents, watermelon (PWM) and water chestnuts (PWC), were chemically processed with different chemicals as modifying agents for the determination and assessment of their adsorption ability for the removal and clearance of harmful, venomous, and pernicious Congo red (CGR), as an acidic nature anionic dye, from the aqueous system. In successive batch experiments, the citric acid-treated peels CPWM and CPWC have shown more promising adsorption performance than their raw and untreated peel counterparts due to the availability of additional adsorption active binding sites evidenced through FT-IR and SEM characterizations. In the Langmuir and Temkin models, the correlation coefficients (R^2) for the adsorptive removal of CGR on CPWM, PWM, CPWC, and PWC are very close to unity, 0.99 for each case of adsorption performance. Furthermore, the q_{max} nonlinear statistical results for the elimination of CGR on citric acid-treated adsorbents (CPWM and CPWC) are 8.3 and 7.95 mg/g whereas for their unmodified forms (PWM and PWC) are 2.23 and 4.32 mg/g, respectively, reflecting homogenous and monolayer adsorption mechanism. The greater values of B_T 1.4 and 1.3 J/mole, for adsorptive removal of dye on CPWM and CPWC, respectively, as compared to their unmodified forms PWM and PWC which are 0.53 and 0.55 J/mole, respectively, indicate the stronger adsorbate-adsorbent associations. The mechanism follows the pseudo second order in the better mode, while thermodynamic statics for $\Delta H^{0,}\Delta G^0$, ΔS^0, and ΔE^0, indicate spontaneous and exothermic behavior of adsorption. This study tends to suggest that citric acid-modified adsorbents CPWM and CPWC may indeed be exploited efficiently to eliminate Congo red dye from wastewater.

1. Introduction

Water, as a universal solvent, is able to dissolve more substances than any other liquid on earth and is unsafe and solely vulnerable to pollution. Toxic substances from agriculture, the domestic sector, and factories readily dissolve into and mix with it, which makes it more difficult for people to access safe drinking water and increases the risks of waterborne diseases. In Pakistan, gastrointestinal illness accounts for 45 percent of newborn mortality, whereas overall, 90 percent of infections are due to waterborne diseases [1–3]. The dye industry has expanded dramatically globally in recent years. As per the "Color Rankings" of the USA, commercial dyestuffs have approached tens of thousands. Every year, about 6×10^7 kg of dyes are released into the environment in the form of effluents, 80% of those are azo

dyes. Dyes that are hazardous, mutagenic, malignant, tragic, and disastrous are extensively utilized in a wide range of industries, like fabrics, cosmetics, printing, leather, food manufacturing, paper, and plastics, and huge amounts of water containing dye effluents enter water resources, causing severe water pollution. Drinking water containing dye effluents may cause dysfunction of the liver, kidneys, and brain. According to reported data, many workers in the Indian dye industry suffer from skin and lung diseases as a result of drinking dye contaminated water [4]. Aromatic and other organic dyestuffs are one of the most widespread contaminants found in wastewaters from fabric and other anthropogenic sectors. Due to the dyes' harmful effects and exposure in surface water, their removal has received a lot of attention across the world [5]. Dye structures are complex and varied, and according to the third edition of the dye ranking, there are around 5×10^3 distinct kinds of dyes, with over 1,500 of them documented. According to estimates, China has synthesized about 5×10^2 distinct types of dyes [6]. Textile industry wastewater is a major source of persistent organic dye pollution in the aquatic environment and is quite complicated in terms of product diversity, methods, techniques, and raw resources. Various procedures and chemical techniques, including bleaching, coloring, imprinting, and finishing, have been applied to the fabric during manufacture [7]. In the textile industry, a wide range of dyes, chemicals, and dye intermediates are used to impart desired properties on fabrics. Therefore, the effluents generated by their wastewater, untreated or partially treated, pose a severe and alarming threat to aquatic life as well as mankind. Various treatment strategies have been adopted in this regard, but they are very complex and complicated to manage, and they consume a lot of expensive chemicals, which raises the operational costs. These include the electrochemical oxidation, solar photo Fenton process, reverse osmosis, membrane, and nanofiltration [8, 9]. Another problem related to these method is continous sludge production [10]. Therefore, it is necessary to formulate a revolutionary and innovative treatment approach that is effective for this sort of contaminated water in terms of fulfilling increasingly stringent discharge limits while still meeting the criteria of total dye removal from aqueous solutions. Hence, adsorption on agrowastes is a premier process of eliminating toxins, noxious, and malignant colorants and auxiliaries from wastewater [11, 12]. Its advantages over other techniques are that it is eco-friendly and easily handled, and raw agrowastes are easily and abundantly available everywhere locally. To enhance the effective adsorption ability, the agrowaste biomass is chemically treated with different chemical modifying agents, and the most suitable and appropriate one was selected for bulk amendments of surfaces of adsorbents [13, 14]. Two agrowaste peels of watermelon and water chestnuts were selected after deep study and literature review of previous reported adsorbents. The performance and efficiency of chemically treated adsorbents are checked and tested by the removal of anionic, toxic, carcinogenic, and hazardous Congo red as model acid dye, and the statistical results are analyzed by comparing them with previously reported data listed in Table 1.

2. Materials and Methods

2.1. Chemicals and Equipment. The chemicals utilized in this investigation include organic compounds such as Congo red dye ($\lambda(\max) = 498$ nm), tartaric acid, lactic acid, citric acid, EDTA, urea, thiourea, methyl orange, phenolphthalein, methyl and ethyl alcohols, 2-propanol, and propanone. The other substances used are caustic soda, soda ash, sodium bicarbonate, sodium chloride, potassium chloride, potassium iodide, and solid iodine, whereas hydrochloric acid, sulfuric acid, and nitric acid were also used to provide acidic media. Pyrex glassware was used for the experiments conducted. Erlenmeyer flasks (100 mL and 500 mL), measuring flasks (100 mL, 500 mL, and 1000 mL), funnels, china dishes, pipette, burette, and beakers were included (100 mL, 200 mL, 500 mL, and 1000 mL). The equipment was washed with an H_2CrO_4/H_2O solution and sterilized in an electric oven at 70°C for half an hour before use.

2.2. Preparation and Characterizations of Adsorbents. Both selected adsorbent peels of watermelon and water chestnuts were obtained locally and dried in sunlight for ten days. After that, they were ground by an electrical grinder and sieved to 70 mesh, washed with distilled water to remove entrapped dust particles as impurities, and dried in an electrical oven at 80°C for 72 hours [15–17]. These prepared peels of adsorbents were labeled "PWM" for peels of watermelon and "PWC" for peels of water chestnuts. These were stored in bulk in polythene bags for further use in experimental work. These are also characterized and evaluated by performing Boehm titration to find the adsorbent sites' behavior (acidic or basic) [18], I_2 titration, moisture and ash content, elemental analysis, volatile matters, measurements of porosity and bulk density ratio, and pH of their raw forms [19–21] and are tabulated in Table 2. To measure the *pH*, 1 g of each PWM and PWC was placed in 40 mL of deionized water in 200-mL flasks separately and stirred for one hour continuously. The pH was measured by using pH meter after stabilization of sample mixtures [22]. Acid-base titrations have been performed to calculate the net surface charge of adsorbent materials using the point of zero charge (pH_{pzc}). To determine the *point of zero charge*, 0.8 g of each PWM and PWC was separately added to 200 mL of 25 ppm sodium chloride solution in two sets of ten Erlenmeyer flasks labeled pH (1 to 10). The initial pH of each solution was adjusted by using NaOH and HCl solutions by using a pH meter. After 10 hours, the final pH of each sample was measured at 30C. Afterward, the difference in change in pH between the initial and final was determined to measure the point of zero charge graphically. If $pH_{(adsorbent)} > pH_{pzc}$, then, the adsorbent surface is even more negatively charged, and the basic dye cations are more preferentially coupled to negatively charged adsorbent interfaces and vice versa [23, 24].

To determine the *bulk density* of PWM and PWC, a density bottle with a lid was weighed (Wi), then filled with distilled water, and weighed again (Wf). By subtracting the (Wi) from the (Wf), the mass of water was calculated. The volume of a density bottle was calculated from Equation (1), where d is the density of water and W is the mass of

Table 1: A comparison of the adsorption capacity of adsorbents with previous reported research work.

Adsorbents utilized	Adsorption capacity (mg/g)	References
Pinus roxburghii sawdust	5.8	[88]
Solanum tuberosum peels	6.9	[89]
Euroamerican poplar biomass	8.0	[90]
Activated carbon from palm tree fiber	9.79	[91]
Carbon from water *hyacinth* leaf	13.9	[92]
Kaolinite	5.0	[93]
Liagora farinose	7.0	[93]
Kaolinite modified by Liagora farinose macroalgae	10	[93]
Roots of Eichhornia crassipes	1.58	[94]
Citric acid-activated peels of watermelon (CPWM)	*8.3*	*This investigation*
Citric acid-activated peels of water chestnuts (CPWC)	*7.95*	*This investigation*
Unactivated raw peels of watermelon (PWM)	*2.23*	*This investigation*
Unactivated raw peels of water chestnuts (PWC)	*4.32*	*This investigation*

Table 2: Physicochemical characterizations of raw adsorbents.

Parameters assessment	PWM	PWC
pH	5.9	5.5
Porosity (%)	0.19	0.09
Moisture contents (%)	8.36	7.72
Ash contents (%)	3.33	1.92
Bulk density ($g\,cm^{-3}$)	1.24	0.48
Particle density ($g\,cm^{-3}$)	0.49	0.6
Volatile organic components (%)	17.8	25.6
Iodine number ($mg.\ g^{-1}$)	13	15
Carboxylic acids (milli moles)	1.9	1.4
Surface basic sites (milli moles)	0.98	0.51

water. Then, a specific amount of each sample was taken in a density bottle and reweighed to measure the volume of the sample. By using Equation (2), the bulk density of both PWM and PWC was determined [25].

$$V = d \text{ x } W, \tag{1}$$

$$\text{Bulk density of PWM and PWC} = \frac{\text{Mass of wet sample peels}}{\text{Volume of sample peels}}, \tag{2}$$

where V_s is the volume of sample adsorbent and d_w is the density of water, whereas the *porosity* of each adsorbent sample was determined using the following equation:

$$\text{Porosity} = \frac{\text{Volume of voids (Vv)}}{\text{Total volume of cylinder (Vt)}}, \tag{3}$$

where the void volume was calculated by the difference between total volume of cylinder for dry density and volume of the each sample adsorbent from Equation (3).

For the determination of porosity, appropriate quantities of each sample PWM and PWC were weighed (G_s), then dried in oven for 3 hours at 100°C to remove the entrapped moisture, and reweighed and labeled as (M_s). The volumes and porosity of each adsorbent were calculated by as follows [26, 27]:

$$\begin{aligned} \text{Vs}\left(cm^3\right) &= \frac{M_s}{G_s} d_w, \\ \text{Porosity} &= \frac{\text{Volume of voids (Vv)}}{\text{Total volume of cylinder (Vt)}}, \end{aligned} \tag{4}$$

where V_s is the volume of each sample PWM and PWC and d_w is density of water. The void volume was determined by the difference between total volume of cylinder for dry density and volume of the each sample adsorbent from the following equation:

$$\text{Volume of Void(Vv), cm}^3 = V_t - V_s. \tag{5}$$

To determine the *ash contents* 1 gram of each PWM and PWC was placed in crucible and ignited at 500°C for three hours and then cooled and reweighed. The following equations were used to determine the *percentage ash content* [28, 29] and the *volatile organic components*, respectively [30].

$$\begin{aligned} \text{Ash content percent} &= \frac{\text{Weight of ash (g)}}{\text{Weight of sample (g)}} \times 100, \\ \text{Volatile organic contents (\%)} &= \frac{W_2(\text{g}) - W_1(\text{g})}{W_2(\text{g})} \times 100, \end{aligned} \tag{6}$$

where W_1 is the ash weight and W_2 is the dry weight of each adsorbent.

To determine the *iodine number* of PWM and PWC, 1.35 g of iodine crystals and 2.05 g of potassium iodide were dissolved to prepare a stock solution. 0.5 g of each adsorbent,

PWM and PWC, was placed in 10 mL of HCl with conc. 5%V/V in two separate Erlenmeyer flasks and stirred for 60 minutes along with the addition of iodine solution and filtered. Afterward, 10 mL of each filtrate was titrated by using 0.1 M $Na_2S_2O_3$ as a standard solution, and the following equation was used to calculate the adsorbed iodine by each sample, PWM, and PWC:

$$\text{Iodine number}\left(\text{mg.g}^{-1}\right) = \frac{(B-S)}{B} \times \frac{V.M}{W} \times 253.81, \quad (7)$$

where the molar mass of I_2 is 253.81 gmol^{-1}, W is the mass of adsorbent, and B is the volume of iodine solution without adsorbent sample, while S is the sample solution. V and M are volumes of filtrate and molar volume of I_2 solution, respectively [31, 32].

Boehm titration was conducted to determine the various types of functional groups on the interfaces of both adsorbents. 0.4 gram of each PWM and PWC was placed separately in 30 mL solutions of 0.1 M HCl, 0.1 M sodium hydroxide, 0.1 M sodium carbonate, and 0.1 M sodium hydrogen carbonate, respectively, and each sample was sealed with aluminum foil and placed at 30°C for 10 hours and then filtered. For filtrates containing excess unconsumed washing soda, baking soda, or caustic soda, 10 mL of each filtrate was titrated against a standard solution of 0.1 M HCl to determine the number of carboxylic, phenolic, and lactone groups, and 0.1 M NaOH to assess the number of basic groups such as $-NH_2$ groups on each PWM and PWC [33, 34].

Therefore, the adsorption of anionic dye molecules like Congo red dye (CGR^-) is highly dependent upon the pH of the solution due to the protonation and deprotonation of COOH moieties on the interfaces of adsorbents [35, 36]. The chemical structure of Congo red dye is depicted in Figure 1 [37].

2.3. Optimization of Adsorbent Performance by Processing with Various Modifying Agents. The adsorbents' performance and efficiency were tested by using different chemicals, as depicted in Section 2.1. For this purpose, the solid phase modification is carried out by using an adsorbent/chemical ratio of 9 : 1 and is elaborated schematically below in Figure 2(a) [38].

The soaking of each adsorbent (50 g) in various organic solvents (200 mL) for 24 hours at room temperature was also conducted, as well as solutions of alkali and inorganic acids, which were also utilized for the chemical processing of PWM and PWC. Thus, chemically modified PWM and PWC were prepared and tested for their adsorption performance by maintaining the optimized operational conditions for CGR as the model dye in this research approach [39]. The most suitable optimized modifying agent for chemical modification of PWM and PWC was selected by performing repeated adsorption experiments. The chemically treated adsorbents were washed with distilled and deionized water to remove entrapped unreactive modifying agent and dried at 80°C in an electrical oven for twenty-four hours and sealed in plastic jars for further adsorption experimental study. The modified adsorbents were characterized by FT-IR and SEM to find the amendments to their surface morphology. Tricarboxylic organic acid-treated adsorbents have shown the highest adsorption of CGR from aqueous solution. Their schematic illustration and the evaluation after chemical treatment with citric acid are shown in Figure 2(b) [40].

2.4. Batch Experimentation on the Adsorption Mechanism. To investigate adsorption mechanism and for optimizing operational parameters, CGR removal with raw PWM and PWC was monitored. Chemically treated watermelon peels (CPWM) and water chestnut peels (CPWC) were used. Experiments on each operational parameter were carried out in four sets of Erlenmeyer flasks, with each set containing 10 to 12 flasks depending on the requirement. All the experiments were highly specific and dependent on operational conditions: adsorbent dose in ten equal divisions was utilized from 0.2 to 2.0 g, time of contact was examined from 5 to 60 minutes, with a gap of five minutes), temperature exploration in eight equal intervals between (10–80°C), impact of the initial as well as final pH between 1–10 and concentration of CGR solution, and speed of agitation (25–250 rpm) with ten equal intervals. Isothermal and kinetic modeling experiments are also performed by considering the optimized operational conditions, and the results are compared with the previous reported investigations listed in Table 1 on the adsorption of Congo red dye on different adsorbents from the aqueous environment. For further evaluation and interpretation of the validity of equilibrium data and performance of adsorption, the thermodynamic parameters like variation in enthalpy, entropy, energy of activation, and Gibbs free energy of each adsorption experiment were determined.

3. Results and Discussions

3.1. Assessment of Chemically Modified Adsorbents Using Various Modifying Agents. The performance of both chemically modified (PWM and PWC) adsorbents in terms of adsorption capability is assessed using a variety of modifying agents, as shown graphically in Figure 3.

After a series of experiments, it was found that citric acid-treated cellulosic biomass (PWM and PWC) performed better, with the highest CGR adsorption results, and their schematically surface amendment with an increase in COOH through different associations on their surface interfaces is elaborated in Figures 2(a) and 2(b). The chemically modified peels of adsorbents (CPWM and CPWC) were prepared as described in Section 2.3 and stored in plastic jars. It was significant to note that throughout the experimentation, chemically modified adsorbents developed quick adsorption equilibrium at low pH (4-6) due to an increase in protonation on the adsorbent-interface, resulting in more electrostatic associations with anionic dye molecules [CGR^-] in the aqueous environment.

3.2. FTIR Analysis. Results of FTIR analysis for all adsorbents before and after removal of dye are presented in Figures 4–6.

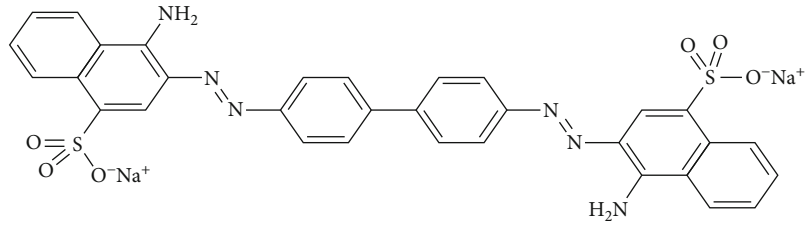

Figure 1: Chemical structure of Congo red dye.

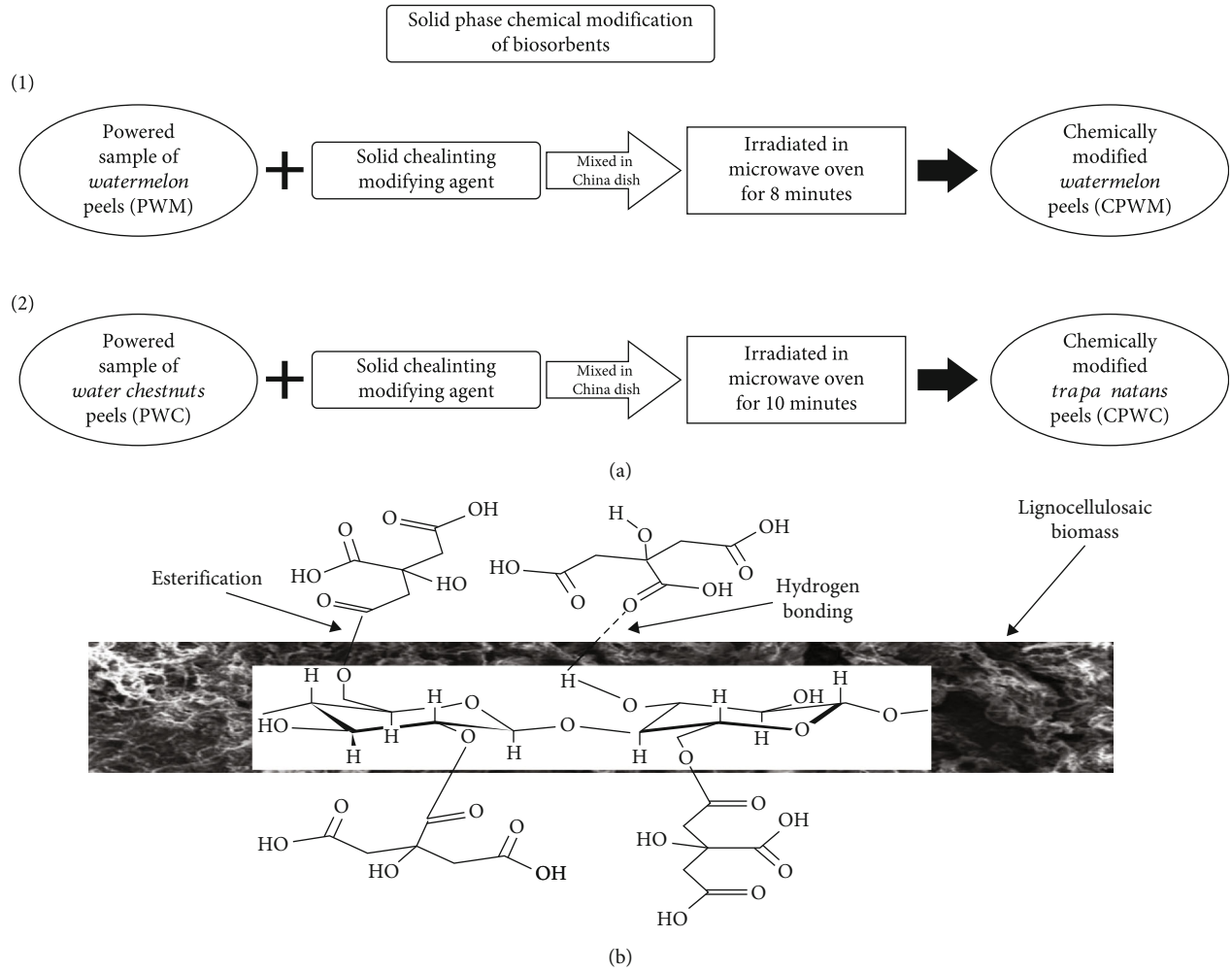

Figure 2: (a) Chemical modification scheme of adsorbents. (b) Illustration of chemically treated adsorbent.

3.2.1. FT-IR Screening of Raw Adsorbents. Figures 4(a) and 4(b) illustrate the FT-IR spectra of raw and unmodified adsorbents PWM and PWC, respectively. The moieties for alcoholic functional groups (OH) are depicted in Figure 4(a) by the frequencies at 3775–3600 $cm^{-1}$and 2900 cm^{-1} [41] and Figure 4(b) by the wavenumbers at 3685–3550 cm^{-1} and 3870 cm^{-1}, respectively. The wavenumbers at 3300 cm^{-1} and at 1720 cm^{-1} in Figure 4(a) and at 3285.5 cm^{-1} and 1685 cm^{-1} in Figure 4(b) represent the OH for carboxylic acid groups, respectively. The peaks at 1720 cm^{-1} and at 1685 cm^{-1} are the signals for C=O groups for COOH moieties [42] in PWM and PWC, respectively. During the study of literature, it was observed that these groups are responsible for the electrostatic associations of the dye molecules during the adsorption mechanism [43].

3.2.2. FT-IR Assessment of Acid-Modified Adsorbents. Figures 5(c) and 5(d) elaborate FT-IR analysis of the citric acid-chelated PWM and PWC adsorbents.

The wavenumbers 3860–3720 cm^{-1} and 3890–3700 cm^{-1} correspond to the chemical interactions of citric acid molecules with OH groups via chelation on the interfaces of

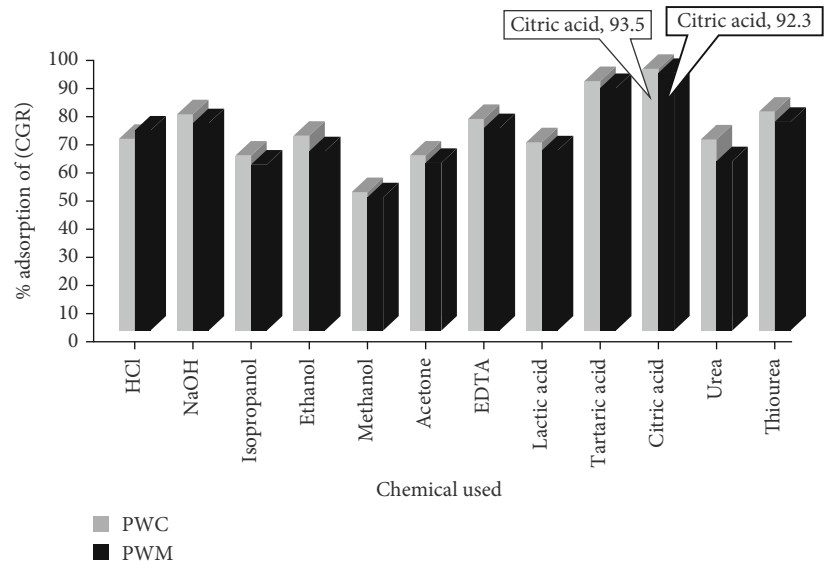

Figure 3: Comparative optimization performance of chemically processed adsorbents with different modifying agents.

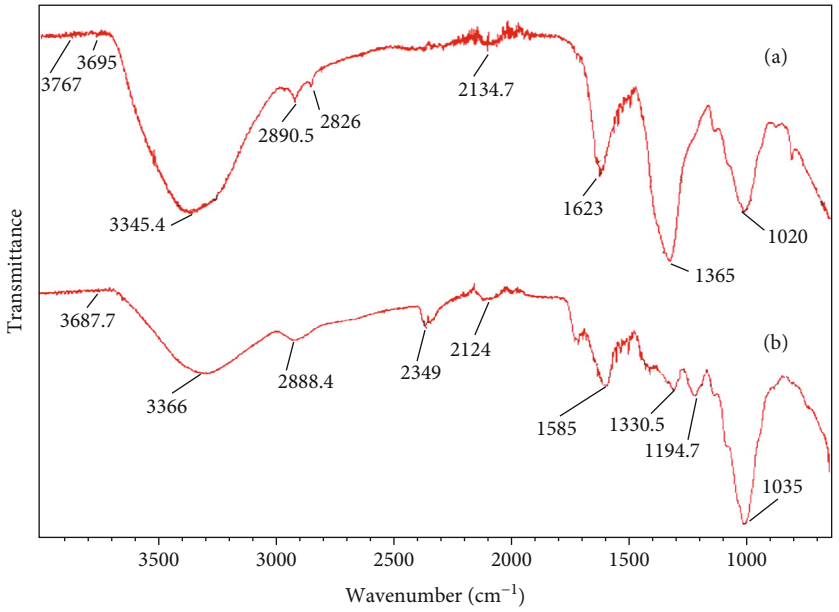

Figure 4: Comparative FT-IR characterization of native adsorbents ((a) PWM and (b) PWC).

CPWM and CPWC, as indicated in Figures 5(c) and 5(d), respectively, providing additional adsorption active sites to interfere with CGR molecules during the adsorption process. The peaks at 3300 and 3250 cm^{-1} depicted OH groups for COOH moieties, while at 2915 cm^{-1} and 2880 cm^{-1} were signals for the presence OH groups of alcohols in CPWM and CPWC, respectively. The strong peaks at 1705 and 1660 cm^{-1} evidenced the carbonyl groups of COOH on the interfaces of CPWM and CPWC [44], which might be responsible for dye molecule affiliations due to their polarity, whereas signals at 1350 and 1325 cm^{-1} indicated OH (bending) for alcohols on the surfaces of CPWM and CPWC, respectively [45, 46].

3.2.3. FT-IR Analysis after Adsorption of CGR on Acid-Modified Adsorbents. Figure 6 illustrates the FT-IR evaluation after the adsorption of CGR on chemically treated adsorbents.

The frequency range at 3840-3690 cm^{-1} and 3900-3670 cm^{-1} represents hydrogen bonds between (>C=O) of carboxylic acid and (>NH_2) of CGR, as well as (OH) of tricarboxylic acid and lone pairs on (NH_2) of CGR, respectively [47], under the influence of the low initial pH range between 5 and 6, depicted in Figures 6(f) and 6(h) for CPWM and CPWC, respectively, whereas in Figures 6(e) and 6(g) for PWM and PWC, respectively. This has obviously shown good adsorption performance of CPWM and CPWC due to amendment of surface morphology as compared to their

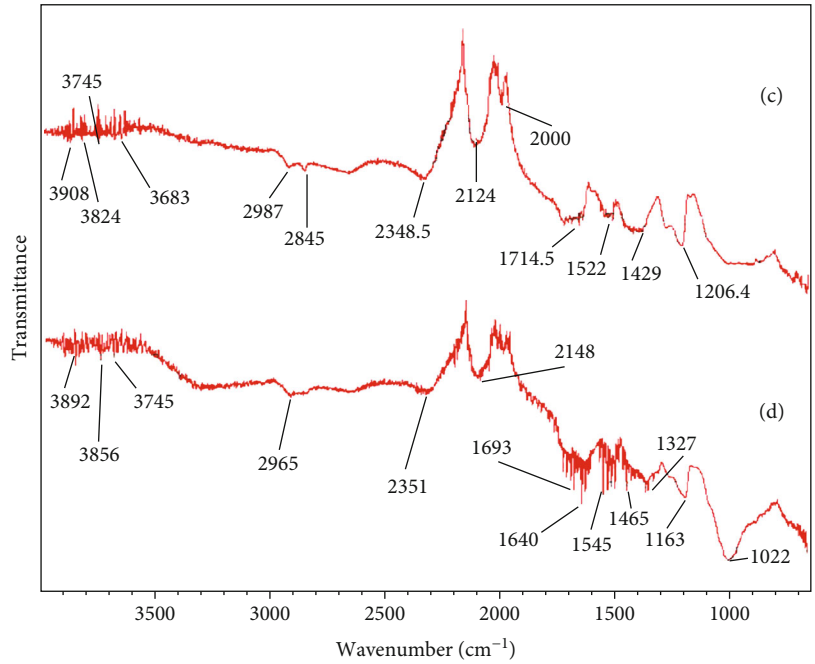

Figure 5: Comparative FT-IR characterization of citric acid-treated adsorbents ((c) CPWM and (d) CPWC).

raw and unmodified forms. The adsorption performance of CGR was directly linked to the influence of interactions due to the protonation of COOH on the interfaces of each CPWM and CPWC. The intermolecular associations between CGR and -OH of COOH moieties are also depicted at the wavenumbers 2880 and 2820 cm^{-1} in Figure 6(f) and 2800 and 2700 cm^{-1} in Figure 6(h), respectively. Peaks at 1680 cm^{-1} in Figure 6(f) and 1650 cm^{-1} in Figure 6(h) indicate the possibility of oxime formation between (>C=O) of COOH on adsorbent surfaces and NH_2 of CGR molecules from aqueous solution. As a result, the citric acid modification of both adsorbents performed more efficient and faster adsorption processes than their raw and native forms [48, 49].

3.3. SEM Analysis. Figure 7(a) represents the screening electron micrograph of native, unprocessed PWM. This includes empty spaces, relatively small, imbedded bouts of depression, and thick spiral clusters, while Figure 7(b) demonstrates its citric acid-treated modified form (CPWM), which has been transformed into flannel, flossy, blocky, wavy, and fluffy objects with varying increased numbers of adsorption binding sites for effective and quicker removal of acid dye (CGR) from aqueous solution. Figure 7(c) displays raw PWC with stuffed fibrous forms, holes, and gaps, whereas Figure 7(d) reveals amended arrangements of its citric acid-modified form (CPWC) with random cylindrical, blocky, and cone-like structural arrangements having a larger surface area. This indicates that the surface topography of PWC has indeed been altered. It is also evidenced by FT-IR characterization, resulting in the provision and promotion of additional adsorption binding sites for the adsorptive exclusion of CGR from the water system.

Figure 7(e) represents the SEM micrograph after the adsorption of CGR on CPWM. It is obviously different morphologically from the CPWM due to its appearance as threadlike, zigzag, highly wavy, fibroid, stringy, and tough, reflecting the good and more percentage adsorption of CGR. Figure 7(f) depicts SEM images of CPWC after CGR adsorption, with a texture resembling thick, coriaceous, tough, cloggy, disk-like, hardened, and manifold, indicating more dye adsorption.

3.4. Optimization of Operating Factors. Operational parameters for the assessment of adsorption efficiency of CGR on each PWM, PWC, CPWM, and CPWC were optimized experimentally as under.

3.4.1. Optimization of Biosorbents Dosage. Biosorbent dosage has a significant impact on the efficiency of the adsorption mechanism. The experiments were conducted in four sets of 250-mL Erlenmeyer flasks, and each set included ten flasks containing 25 ppm CGR with a volume of 25 mL.

The biosorbent dosage range of 0.2-2 g was studied with a difference of 0.2 g for each PWM, CPWM, PWC, and CPWC at 40°C, initial pH 4, and 125 rpm agitation speed. The maximal adsorptive removal rate of acid dye was established experimentally as follows: 71.4% removal of CGR on 0.8 g of PWM and 95% removal of CGR on 0.8 g of its acid-treated form, CPWM, whereas 75.7% eradication of CGR on 0.8 g of PWC and 95% on 1.0 g of CPWC illustrated in Figure 8. The decrease in adsorption performance with an increase in adsorbent dosage is due to the rapid establishment of equilibrium between CGR and at the interfaces of each adsorbent due to the many unoccupied adsorption sites as depicted in Figure 8 [50]. The optimized 0.8 g adsorbent dosage for each adsorption case was selected in this investigation.

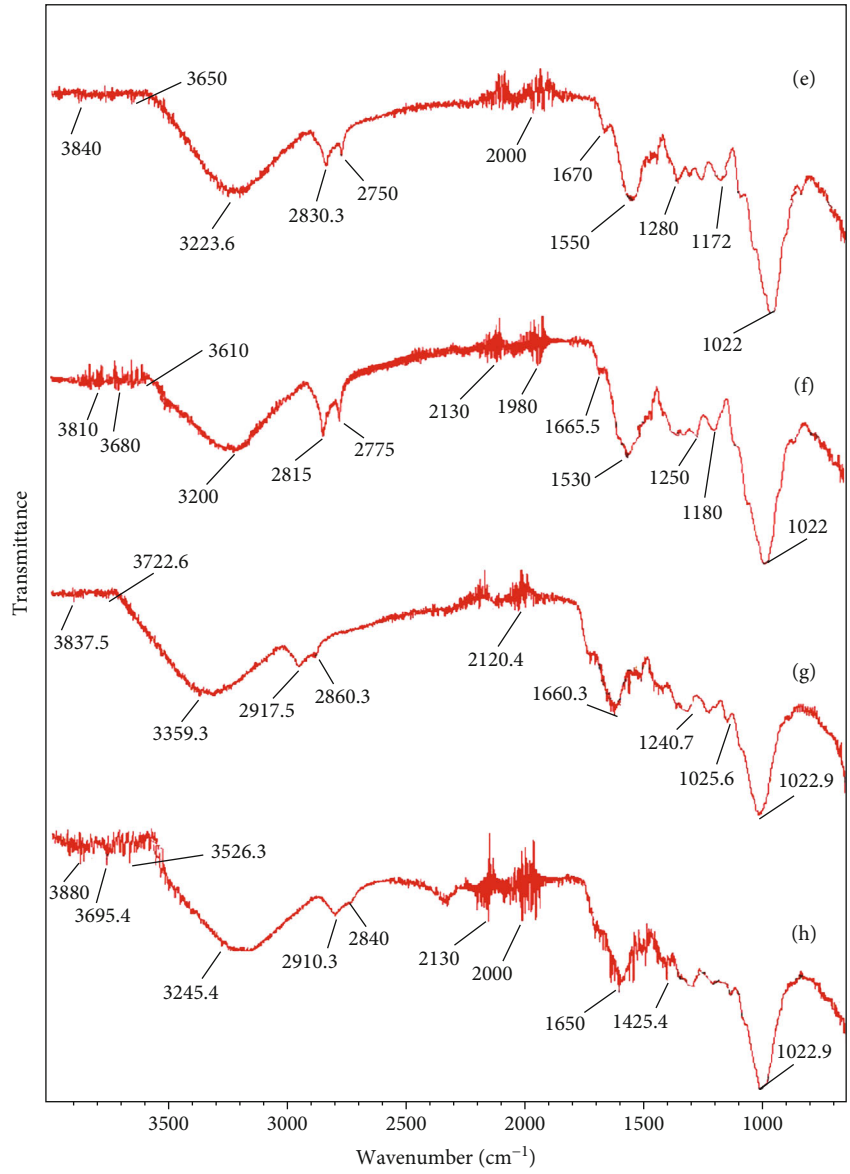

Figure 6: Comparative FTIR analysis after adsorption of CGR on chemically modified adsorbents ((e) CGR + PWM, (f) CGR + CPWM, (g) CGR + PWC, and (h) CGR + CPWC)).

3.4.2. Optimization of Contact Time Duration. The effectiveness of the adsorption process is equivalent to the number of accessible binding sites on the interfaces of each PWM, CPWM, PWC, and CPWC.

Figure 9 reveals the determination of 84.3% adsorptive elimination of CGR on PWM at 30 minutes and 95% on its acid modification and CPWM at 25 minutes, whereas 75.7% on PWC at 40 minutes and 97.2% on CPWC at 20 minutes after batch mode experiments. The experiments were conducted by using 25 ppm solutions with a volume of 25 mL on 0.8 g of each adsorbent at 40°C, 125 rpm, and an initial pH of 4. Adsorption declines with time by the unit mass of each adsorbent after a specific frequency owing to equilibrium, leaving numerous empty adsorption binding sites unoccupied [51], as shown in Figure 9.

3.4.3. Agitation Rate Optimization. Another important operational parameter that controlled the adsorption rate for the elimination of CGR from water on PWM, CPWM, PWC, and CPWC was the agitation rate (rpm). This factor was investigated at speeds ranging from 25 to 200 rpm, with a 25 rpm variation at 40°C temperature, and an initial pH of 4 on 0.8 g of each adsorbent dosage.

Figure 10 displays the biosorption removal of CGR as follows: 73.5% on PWM at 125 rpm and 97.2% on its citric acid-modified form CPWM at 125 rpm, whereas 75.7% on native PWC at 125 rpm and 92.9% on its amended formulation at CPWC at 125 rpm, indicating the effective adsorption performance of chemically treated adsorbents as compared to their untreated forms. During the experiments, it was found that fast agitation speeds generated a thin layer of

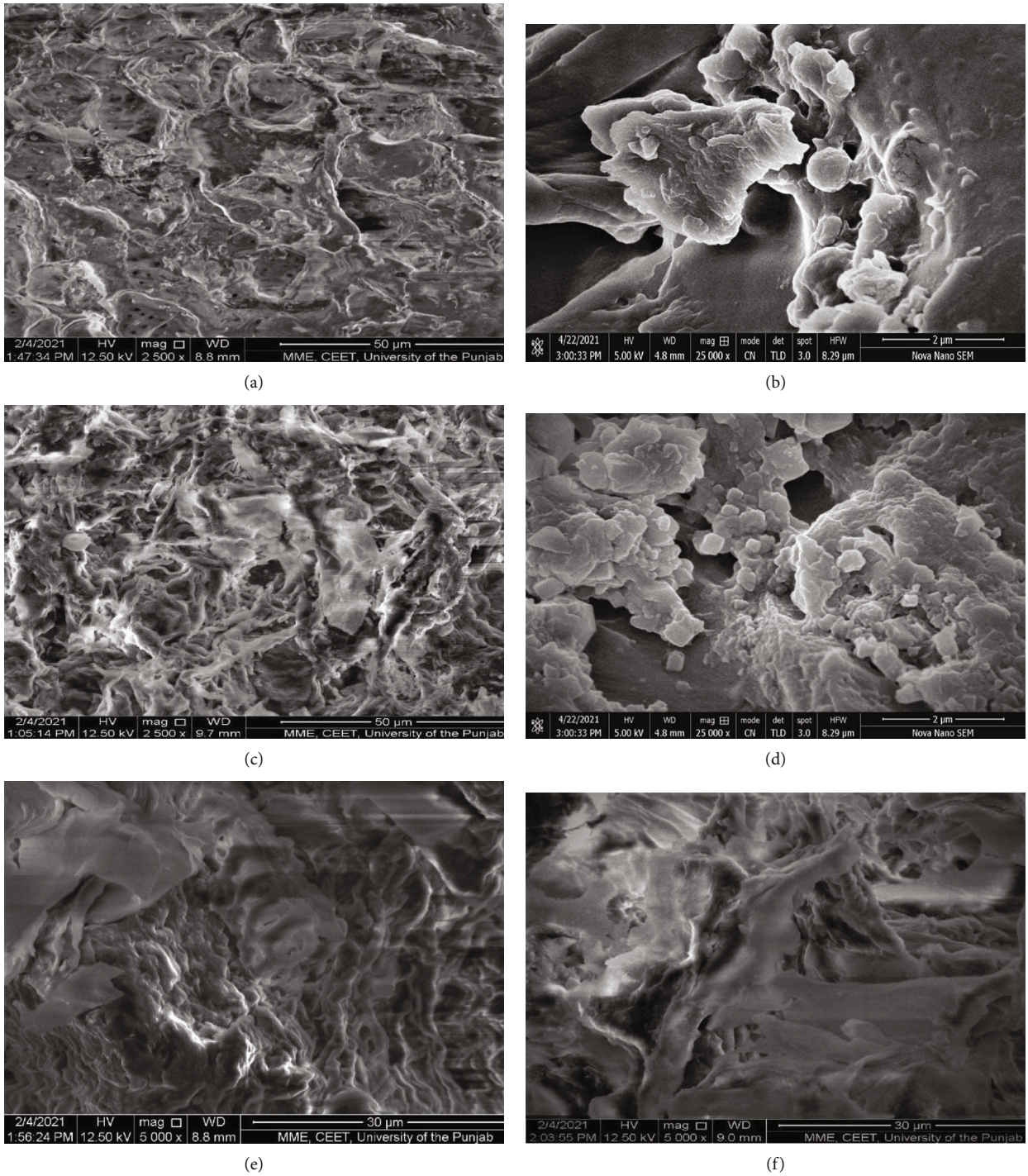

Figure 7: SEM comparison of adsorbents before and after chemical modification as well as dye loading ((a) PWM, (b) CPWM, (c) PWC, (d) CPWC, (e) CGR+ CPWM, and (f) CGR + CPWC).

CGR molecules from the bulk on the surface interface of each adsorbent, which directly decreased the adsorption performance and increased the desorption of CGR [32]. The decrease in percentage adsorption of CGR at high agitation speeds of 125 rpm on CPWM and CPWC and 150 rpm on unmodified adsorbents PWM and PWC is also due to the fast and increased number of collisions of dye molecules on the adsorbent surfaces. The resulting repulsive forces become more operative and significant between free anionic [CGR^-] molecules in an aqueous system and adsorbed CGR molecules on the interfaces of adsorbents [52]. Furthermore, the negatively charged binding sites on the surfaces of adsorbents also repelled the anionic dye molecules during the high agitation rate. Thus, increased agitation rates quantitatively increase desorption of CGR from the interfaces of adsorbents under the influence of the ion exchange mechanism

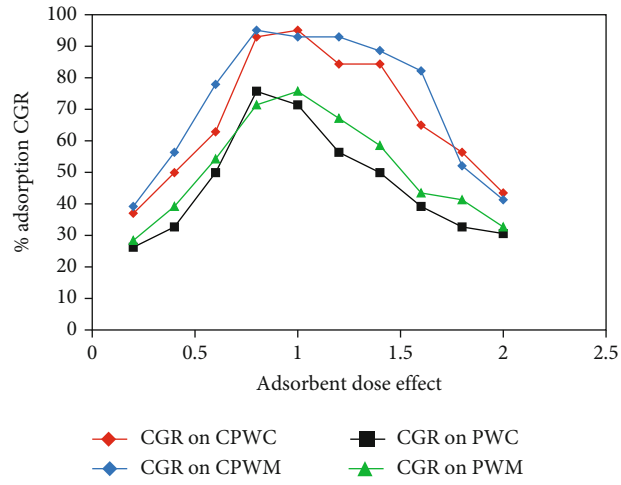

Figure 8: Optimization of biosorbents dosage.

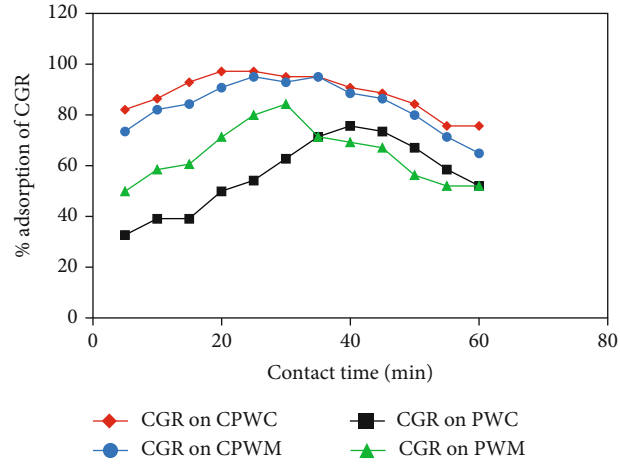

Figure 9: Optimization of contact time.

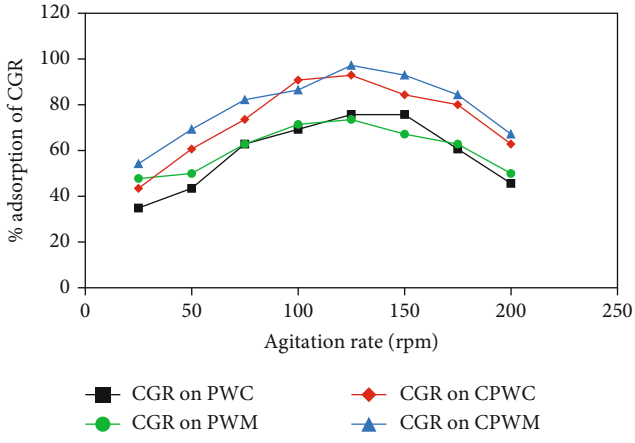

Figure 10: Optimization of agitation rate.

[33]. Therefore, an optimized agitation rate of 125 rpm is determined after repeated experiments for further investigation, as depicted in Figure 10.

3.4.4. Optimization of Temperature for Adsorption Mechanism. Kinetic energy is directly linked with the variation of temperature of the CGR solution and ultimately influences the thermodynamic parameters, resulting in adsorption performance of biosorbents. The biosorption performance was investigated for a temperature range of 10–80°C with a difference of 10°C for 25 ppm CGR solution with a volume of 25 mL on 0.8 g of each biosorbent at 125 rpm and at initial pH 5. A temperature-controlled water bath was employed to keep the temperature stable during the experiment. This experiment was carried out to better understand the physical changes that occur on adsorbents when temperatures rise. To prevent evaporation, the experimental flasks were sealed with Al-foil. The experiment was carried out to better understand the physical changes that occur on adsorbents when temperatures rise.

Figure 11 graphically represents the biosorption results, which are as follows: PWM eliminated 75.7% of CGR at 40°C, and its acid-modified form, CPWM, eliminated 95% of CGR at 30°C, whereas PWC and its acid modification, CPWC, eliminated 80 and 92.9% of CGR, respectively, at 40°C. The adsorption performance decreases after 40°C in each of the cases which can be analyzed in Figure 11. This might be due to devastation, decimation, and disintegration of the structure lignocellulosic biomass of each adsorbent [53]. This behavior can be analyzed for PWM at 60°C which has been shown to have an 80% eradication of CGR, and for PWC, which has shown a decrease in adsorption at 40 to 50°C from 80% to 73.5%, with an afterward increase in adsorption to 80% again at 50 to 60°C. As a result, a temperature of 40°C was determined to be optimal for future adsorption experiments.

3.4.5. Optimization of pH for Adsorption Performance. The adsorption process is specifically correlated to the initial pH of the dye solution [54]. The biosorption potential was examined for a pH range of 1–10, for a 25 ppm CGR solution with a volume of 25 mL on 0.8 g of each biosorbent at optimal temperature, contacting duration, and agitation speed. 0.1 molar of each NaOH or HCl solution was used to regulate pH during the adsorption experiments. Low pH favored protonation at the interface surfaces of each adsorbent PWM, PWC, CPWM, and CPWC, resulting in anions [CGR^-] flowing quickly towards adsorbents, overcoming repulsive forces [55, 56].

The amino groups of CGR get chelated with the COOH moieties on the adsorbent surfaces. During batch experiments, it was discovered that at pH 4-6, the adsorption of CGR molecules was quick and promising, but that with a unit one increase in pH 6-10, the results were unfavorable, which could be due to an increase in deprotonation of COOH moieties on adsorbents providing anionic binding sites, resulting in an increase in repulsion against [CGR-] ions in the aqueous system. Figure 12 illustrates graphically the maximum adsorption elimination of CGR on PWM 82% at pH = 4, on CPWM 95% at pH = 4, on PWC 75.7% at pH 4, and on CPWC 93% at pH 4. As a result, the optimal pH value 4 was chosen for future investigations.

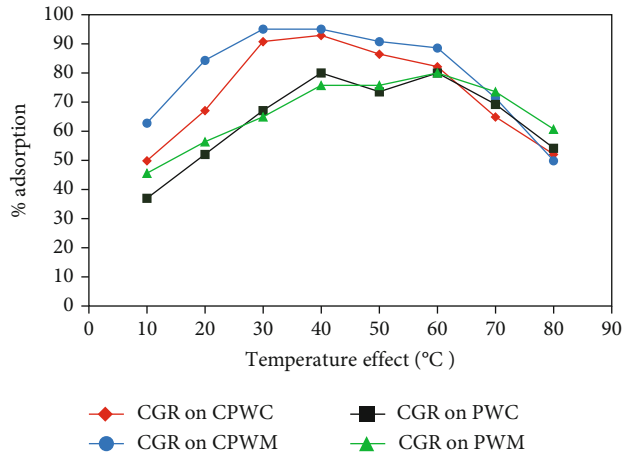

Figure 11: Optimization the effect of temperature.

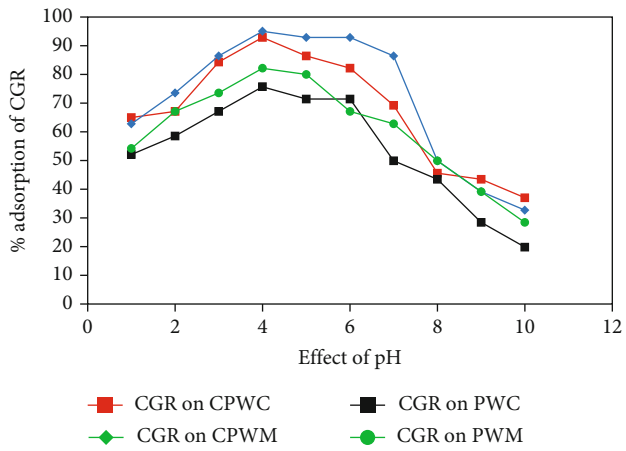

Figure 12: The impact of initial pH on adsorption performance.

3.5. Adsorption Isothermal and Kinetics Investigations. The adsorption of CGR on modified and unmodified adsorbents was investigated by applying Langmuir, Freundlich, and Temkin as well as kinetics models of equilibrium under optimized operational conditions as follows: adsorbent dosage of 0.8 g, initial pH of 4, and 25 ppm CGR solutions with a volume of 100 mL at 40°C and 125 rpm shaking speed.

3.5.1. Interpretation of the Langmuir Adsorption Model. A nonlinear Langmuir isothermal plot (Q_e vs C_e) is expressed in Figure 13. The following equation represents nonlinear form of the Langmuir model [57, 58], while significant Langmuir parameters are tabulated in Table 3.

$$q_e = \left[\frac{b.C_e.q_{\max}}{1+(b.C_e)}\right] (\text{nonlinear}), \tag{8}$$

$$q_e = \frac{(Co-Ce)V}{m}, \tag{9}$$

$$R\,(\%) = \frac{(Co-Ce)}{C_o} \times 100. \tag{10}$$

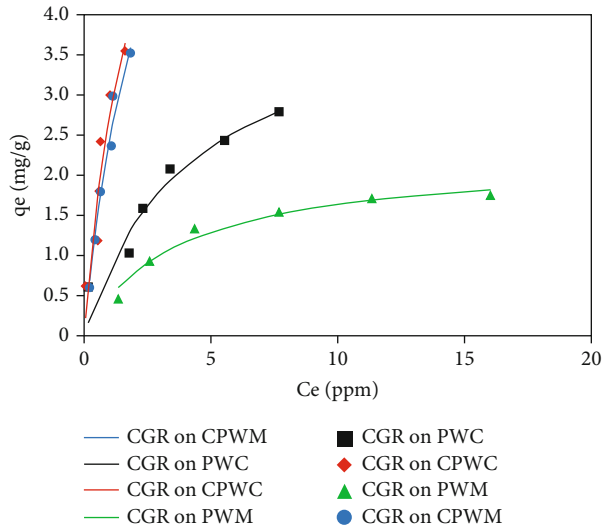

Figure 13: Nonlinear Langmuir isothermal investigation.

The adsorption capacity and percentage removal (R%) of CGR are calculated from Equations (9) and (10), respectively, where qe is the adsorbed quantity of CGR and Ce is the quantity of CGR left after adsorption, while q_m (mg.g^{-1}) is the highest adsorption capacity, and b is (L.g^{-1}) for adsorption energy, whereas in equation (9), V is the volume of adsorbate in dm^3, while (m) is related to the mass of each adsorbent used in experimental work [59]. The correlation coefficients (R^2) for the adsorption of CGR on CPWM, PWM, CPWC, and PWC are 0.999, 0.998, 0.997, and 0.988, respectively, and are closer to unity, while the maximum adsorption capacities ($Q_{\max}$) of both citric acid processed adsorbents CPWM and CPWC are 8.3 and 7.95, respectively, as compared to their unmodified forms, PWM and PWC, which are 2.23 and 4.32 mg/g, respectively, reflecting the suitability and fitness of this isothermal model for the adsorptive eradication of CGR from aqueous solutions. The $q_{\max}$ of present study is compared with the previous reported data in Table 1. The Langmuir constants "b" (adsorption energy) for acid-treated adsorbents CPWM and CPWC are 0.42 and 0.53, which are sufficiently high as compared to unmodified adsorbents PWM and PWC at 0.27 and 0.24 (L.g^{-1}), respectively. These Langmuir constants "b" are calculated from the nonlinear mode of Langmuir isotherm Equation (8), reflecting the more adsorption energy and comparatively stronger forces between dye molecules and interfaces of citric acid-treated adsorbents due to the availability of additional COOH moieties. The nonlinear regression analysis results of this isotherm tabulated in Table 3 express the suitability and fitness of this model on equilibrium data.

These statistics and findings relate to monolayer homogenous adsorption due to a set number of equivalent binding adsorption sites spread on adsorbents surfaces. The standard deviations for PWM, CPWM, PWC, and CPWC are 0.46, 1.003, 0.765, and 1.011, respectively, and are expressed in Figure 14.

Table 3: A comparative nonlinear isothermal studies for the adsorptive removal of CGR.

Parameters for nonlinear isotherms	CGR on CPWM	CGR on PWM	CGR on CPWC	CGR on PWC
Langmuir isotherm				
R^2	0.99	0.99	0.99	0.98
q_{max} (mg. g^{-1})	8.3	2.23	7.95	4.32
b (L.mg^{-1})	0.42	0.27	0.53	0.24
Standard deviations	1.003	0.460	1.011	0.765
ΔG° (kJmol^{-1})	-2.2	-3.2	-1.6	-3.5
RMSE	0.0277	0.0067	0.1189	0.0480
Freundlich isotherm				
R^2	0.99	0.99	0.99	0.99
n	0.729	0.397	0.668	0.495
K_F (mg. L^{-1}) × (L.mg^{-1})$^{1/n}$	2.37	0.633	2.49	1.03
RMSE	0.0002	4.8×10^{-05}	0.0002	0.0001
Temkin isotherm				
R^2	0.99	0.99	0.99	0.99
B_T (J/mole) × (mg.g^{-1})$^{-1}$	1.4	0.53	1.3	0.55
K_T (L.g^{-1})	6.2	2.2	8.0	11.3

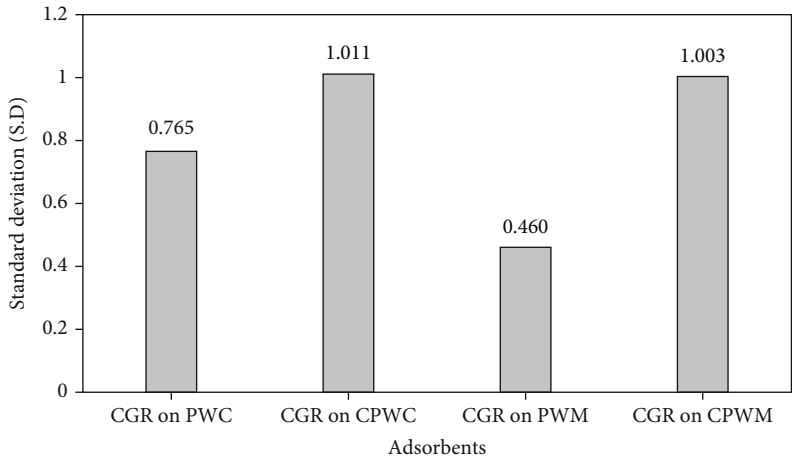

Figure 14: Study of standard deviations.

3.5.2. Interpretation of the Freundlich Isotherm. The nonlinear form of Freundlich isotherm is shown in Equation (11) and is graphically represented in Figure 15. This isothermal model correlates with the surface heterogeneity and potency of biomass towards adsorption of CGR from aqueous solutions [60, 61].

$$q_e = K_F C_e^{1/n}, \tag{11}$$

where Freundlich adsorption constants K_F (mg. L^{-1}) × (L.mg^{-1})$^{1/n}$ are associated with adsorption capacity and n with adsorption intensity. The significant calculated parameters of this isotherm are tabulated in Table 3. The correlation coefficients (R^2) for the adsorptive removal of CGR on PWM and CPWM are 0.99 and 0.99, respectively, while on PWC and CPWC are also 0.99 and 0.99. The higher values of K_F for citric acid processed adsorbents CPWM and CPWC are 2.4 and 2.5 (mg. L^{-1}) × (L.mg^{-1}), respectively, as compared to their unmodified PWM and PWC, which are 0.6 and 1.0 (mg. L^{-1}) × (L.mg^{-1}), respectively, indicating the more surface heterogeneity. The significant parameters are tabulated in Table 3.

3.5.3. Interpretation of the Temkin Isotherm. The heat of adsorption (B_T) of CGR on untreated and chemically treated adsorbent surfaces was linearly reduced as dye molecules [CGR^-] progressively covered their interfaces due to their association with active sites [62, 63].

The Temkin constants B_T and K_T are calculated by using the nonlinear relation shown in Equation (12) [64] and by plotting (q_e vs C_e) as illustrated in Figure 16.

$$q_e = B_T.\ln(K_T.C_e), \tag{12}$$

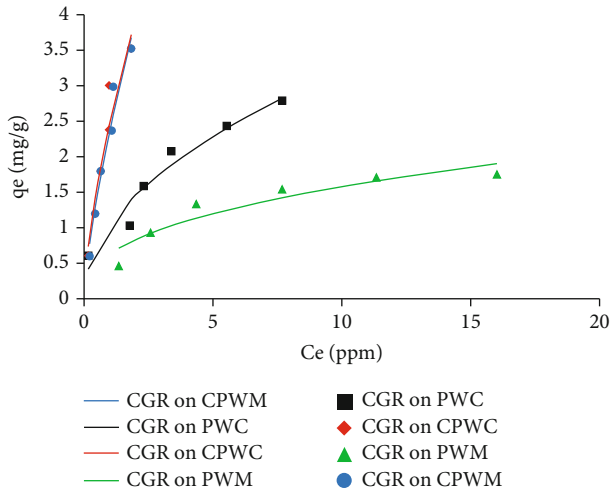

Figure 15: Nonlinear Freundlich isothermal investigation.

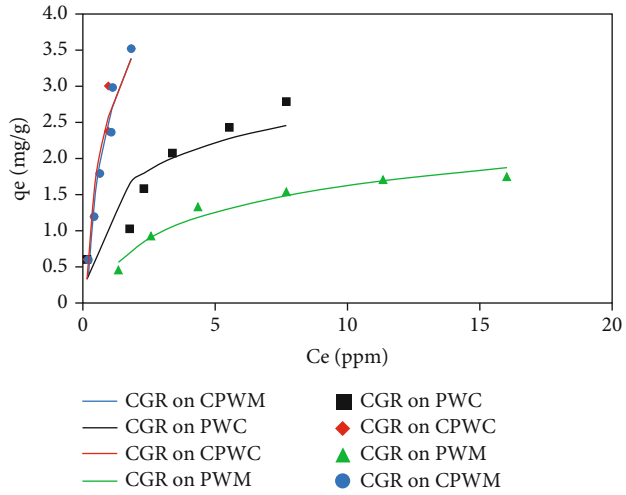

Figure 16: Nonlinear Temkin isothermal investigation.

where $B_T = RT/b$ (kJmol^{-1}) shows the heat of adsorption, while K_T is the equilibrium binding constant. The heat of adsorption (B_T) values calculated from nonlinear Equation (12) are tabulated in Table 3, which determine the nature of the interactions of dye on the surfaces of each modified and unmodified adsorbent [65]. The greater values of B_T of 1.4 and 1.3 J/mole for modified adsorbents CPWM and CPWC, respectively, indicate the stronger adsorbate-adsorbent associations as compared to their unmodified forms PWM and PWC, which are 0.53 and 0.55 J/mole tabulated in Table 3. Furthermore, the nonlinear regression analysis correlation coefficients (R^2) for all adsorbents CPWM, CPWC, PWM, and PWC are very close to unity, indicating the suitability and fitness of the Temkin isotherm.

Heat of adsorption ($B_T < 8$) values for the adsorption during the adsorbate-adsorbent interactions indicating physio-sorption rather than chemisorption [66, 67]. The equilibrium binding constant$K_T$value corresponding to maximum binding energies for adsorption of CGR on CPWM is 6.2 L/g and on PWM is 2.2 L/g, while 8.0 L/g on CPWC and 11.3 L/g on PWC, as tabulated in Table 3, also reflecting suitability and fitting of Temkin isothermal model along with the Langmuir isotherm.

3.5.4. Adsorption Kinetic Investigation

(1) Pseudo First Order. Lagergren nonlinear equation of pseudo first order is displayed in Equation (13), while its graphical plot is shown in Figure 17 [68, 69], and the significant parameters are listed in Table 4.

$$q_t = \left[q_e\left(1 - e^{-k_1 t}\right)\right], \tag{13}$$

where q_e is the equilibrium adsorption capacity (mg/g) and q_t is the adsorption capacity (mg/g) at time (t) min^{-1} and K_1 indicates the rate constant (g.mg^{-1}.min^{-1}) [70].

Figure 16 graphically exhibits a nonlinear plot between (q_t vs t), and the resulting calculated parameters are tabulated in Table 4. The correlation coefficients (R^2) are close to unity and the rate of reaction (K1) for each CPWM, CPWC, PWM, and PWC which are 0.353, 0.0802, 0.078, and 0.160 (per minute). The calculated equilibrium adsorption capacity (*qe*, mg/g) differs from the experimental (*qe*, mg/g) in all acid-modified (CPWM, CPWC) and unmodified (PWM, and PWC) adsorbents, indicating that this kinetic model on equilibrium data is unsuitable for adsorptive removal of CGR.

(2) Pseudo Second Order. Nonlinear relation of pseudo second order proposed by HO and McKay is depicted in the equation as follows [71, 72] and graphically in Figure 18. The effective parameters are tabulated in Table 4.

$$q_t = \left[\frac{\left(k_2.q_e^2.t\right)}{\left(1 + k_2.q_e.t\right)}\right], \tag{14}$$

where q_e is the equilibrium adsorption capacity (mg/g) and q_t is the adsorption capacity (mg/g) at time (t) min^{-1} and K_2 (g.mg^{-1}.min^{-1}) indicates the rate constant of experimental outcomes.

The calculated equilibrium adsorption capacity (*qe*) is nearly close to the experimental equilibrium adsorption capacity (q_e), for the adsorption of CGR on CPWM, PWM, CPWC, and PWC, and is 0.84, 0.452, 0.61, and 0.43 mg/g, respectively, reflecting the fitness of pseudo second-order kinetics on equilibrium data of adsorption [73]. Furthermore, the correlation coefficients (R^2) for adsorptive removal of dye molecules on all acid-modified and non-modified adsorbents are 0.99 close to unity and are listed in Table 4, indicating the well fitness of pseudo second order than the pseudo first-order kinetics mechanism.

To assess the validity of equilibrium data, the root mean square errors for all cases of CGR adsorptive removal are determined using Equation (15) [74], and the percent relative deviation (P) values are calculated using Equation (16) [75] to assess the reliability of the adsorption findings

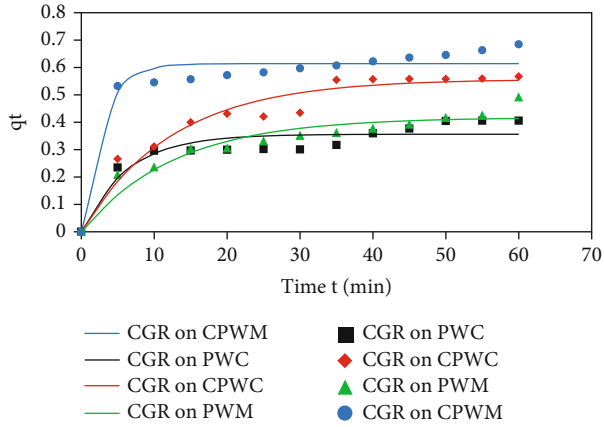

Figure 17: Nonlinear pseudo first-order kinetic study.

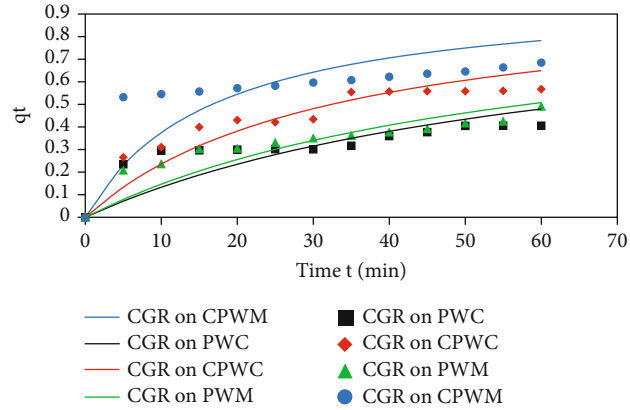

Figure 18: Nonlinear pseudo second-order kinetic study.

Table 4: Nonlinear comparative study of kinetic parameters for detoxification of CGR.

Kinetic adsorption nonlinear parameters	CGR on CPWM	CGR on PWM	CGR on CPWC	CGR on PWC
Pseudo first order				
R^2	0.99	0.99	0.99	0.99
q_e (mg.g^{-1}) (exp.)	0.688	0.513	0.624	0.438
q_e (mg.g^{-1}) (cal.)	0.613	0.417	0.428	0.356
k_1 (per min.)	0.353	0.078	0.0802	0.160
RMSE	0.0014	0.0012	0.0014	0.0014
P	0.823	1.422	0.817	1.76
Pseudo second order				
R^2	0.99	0.99	0.99	0.99
K_2 (g. mg^{-1}.Min^{-1})	0.071	0.038	0.051	0.036
q_e (mg.g^{-1}) (exp.)	0.688	0.513	0.624	0.438
q_e (mg.g^{-1}) (cal.)	0.844	0.452	0.605	0.427
RMSE	1.391	0.003	0.004	0.006
P	-0.0002	0.911	0.228	0.184

tabulated in Table 4. The lowest values for both RMSE and P for second-order kinetics support its appropriateness and fitness over first-order kinetics [76].

$$\text{RMSE} = \sqrt{\sum \frac{\left[q_{e(\text{cal})} - q_{e(\text{exp})}\right]^2}{N}}, \tag{15}$$

$$P = \frac{100}{N} \sum \left[\frac{q_{e(\text{exp})} - q_{e(\text{cal})}}{q_{e(\text{exp})}}\right]. \tag{16}$$

3.6. Adsorption Thermodynamic Investigations. Nonlinear graphical representation of thermodynamic parameters such as enthalpy change, entropy change, Gibbs free energy, and activation energy was also investigated during experiments to authenticate and validate equilibrium data [77]. Temperature changes correlate with the diffusion, kinetic energy, and angular velocity of CGR in the aqueous phase. This property influences the efficiency of the adsorbents for the adsorption removal mechanism of Congo red dye molecules because of the pervious and rubbery, squishy, and porous surface of hemicellulose and adsorbent peels. The statistical results of the calculated thermodynamic parameters ΔG^0, ΔH^0, ΔS^0, and ΔE_a by using Equations (17), (18), (19), and (20) are listed in Table 5 and are graphically represented in Figure 19.

The Gibbs free energy calculated from Equation (17) [53], for the adsorption of CGR on chemically modified adsorbents CPWM (-13.7, -6.67, and -4.95 kJmol^{-1}) and CPWC (-8.95, -5.9, and -4.5 kJmol^{-1}), as compared to their unmodified forms, PWM (-7.4, -5.3, and -4.1 kJmol^{-1}) and PWC (-6.5, -4.8, and -3.7 kJmol^{-1}) at 298, 308, and 318 kelvin temperatures, respectively, suggests that the process is spontaneous in standard conditions. [67].

$$\Delta G^0 = -\text{RT}\, \boldsymbol{ln}\, K_D, \tag{17}$$

$$\ln K_D = \frac{\Delta S0}{R} - \frac{\Delta H0}{\text{RT}}, \tag{18}$$

$$K_D = \frac{C_o - Ce}{Ce}. \tag{19}$$

The distribution coefficient (K_D) was determined from the relation shown in Equation (19), where C_o and C_e are the initial and equilibrium concentrations of CGR solutions, respectively, whereas R is the universal gas constant and T is the temperature in kelvin in Equation (17). The change in enthalpy (ΔH^0) varied between 2.1 and 20.9 kJmol^{-1}, exhibiting physio-sorption, and from 80 to 200 kJmol^{-1}, exhibiting chemisorption [78]. Therefore, exothermic enthalpy changes calculated from Equation (18), for adsorptive eradication of CGR on citric acid-processed biosorbents CPWM is (-145 kJmol^{-1}) and on unprocessed PWM is (-57 kJmol^{-1}), whereas on CPWC is (-76 kJmol^{-1}) and on its raw form is (-48 kJmol^{-1}) indicating the chemisorption adsorption mechanism. The higher the ΔH^0 value for citric acid treated biosorbents in comparison to their raw peels reflecting the

Table 5: Nonlinear comparative study of thermodynamic parameters.

Adsorption of CGR on adsorbents	T (K)	K_D	ΔG (kJ/Mol)	ΔH (kJ/Mol)	ΔS (J Mol^{-1} K^{-1})	Ea (kJ/Mol)
CGR on CPWM	298	0.004	-13.7	-145	443	145
	308	0.074	-6.67			
	318	0.154	-4.95			
CGR on PWM	298	0.05	-7.4	-57	168	57
	308	0.126	-5.3			
	318	0.214	-4.1			
CGR on CPWC	298	0.027	-8.95	-76	225	76
	308	0.099	-5.9			
	318	0.183	-4.5			
CGR on PWC	298	0.074	-6.5	-48	138	48
	308	0.154	-4.8			
	318	0.247	-3.7			

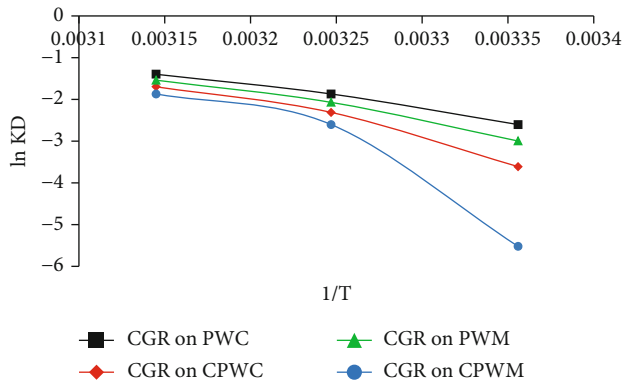

Figure 19: Nonlinear adsorption thermodynamic approach.

tighter adsorbate-adsorbent interactions at their surface interfaces, resulting in the efficient eradication of CGR from the water system. The contortion and deformation at the adsorbate-adsorbent interface associated with entropy change (ΔS^0) is also calculated from Equation (25) [79, 80]. High calculated ΔS^0 for adsorptive removal of CGR by CPWM and CPWC is 443 and 225 Jmol^{-1} K^{-1}, respectively, as compared to 168 Jmol^{-1} K^{-1} for PWM and 138 Jmol^{-1} K^{-1} for PWC, respectively, listed in Table 5.The increased energies of activation (ΔE_a) calculated from Arrhenius Equation (20), for the removal of CGR from the aqueous environment on acid-treated CPWM and CPWC, are 145 and 76 kJmol^{-1}, respectively, whereas on PWM and PWC are 57 and 48 kJmol^{-1}, respectively, indicating the fast and efficient adsorptive removal of CGR on citric acid-treated adsorbents [81]. The adsorption capacity q_{max} of present investigation is compared with the previous reported data in Table 1.

$$\ln K = \ln A - \frac{E_a}{RT}. \quad (20)$$

3.7. Adsorption Mechanism. Various new additionally provided functional groups including, -OH, –COOH, >C=O, NH_2 on the surfaces interfaces of chemically modified adsorbents have been contributed a vital and central role in the adsorptive eradication of CGR from aqueous solutions [82, 83]. CGR, being an acidic as well as an anionic dye, was repelled by the anionic adsorption sites on adsorbents relatively at the high initial pH of the solutions. Protonation of adsorbents at pH 4-5 favors and influences the anionic molecules [CGR$^-$] of dye propelled towards the active adsorbent sites of adsorbents, resulting in an increased rate of adsorption performance as schematically shown in Figure 20.

After the assessment and evaluation of numerous experimental results, it was concluded that the adsorption mechanism is primarily linked with both chemisorption and physio-sorption. Chemisorption is associated with chelation reactions between the amino groups (NH_2) of CGR molecules and excessive as well as additionally provided carboxylic acid groups (COOH) to citric acid-treated adsorbents [84], whereas physio-sorption is linked with electrostatic interactions such as hydrogen bonding between >C=O of carboxylic acid moieties on adsorbents and partially positively charged hydrogen atoms (H-N-H) of CGR in aqueous solutions [85], as illustrated in the proposed mechanism in Figure 20.

3.8. Desorption. Desorption of CGR from exhausted adsorbents was conducted by using different eluents which have capability to break the adsorbate-adsorbent interactions for their further use and to assess the change in their adsorption performance. The most appropriate and promising desorbing agent, 0.1 M NaOH, has been used for CGR desorption from the used adsorbents [86], whereas the high concentration has been avoided because it could damage and degrade the alignment and crystalline structure of cellulosic biomasses, causing a drop in their adsorption performance [87]. The maximum desorption CGR recorded in this

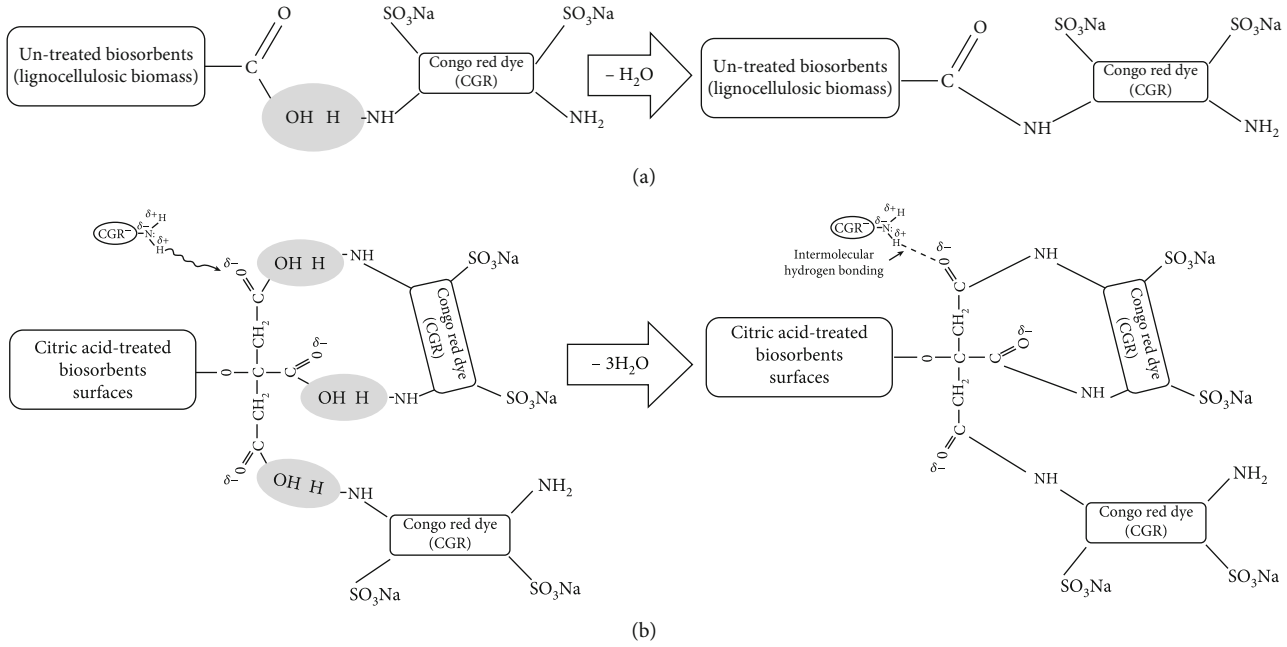

Figure 20: Schematic mechanism of adsorption for CGR ((a) adsorption on untreated adsorbents and (b) adsorption on citric acid-treated adsorbents).

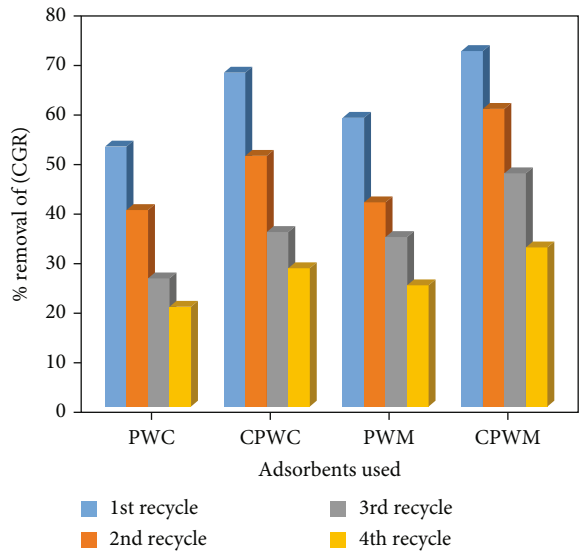

Figure 21: Study of comparative recycling of adsorbents for the degradation of CGR.

investigation was 87% for CPWM, 85% for CPWC, 80% for PWM, and 75% for PWC.

Figure 21 shows that the adsorptive performance of adsorbents decreased with an increase in the number of cycles for each adsorbent. Desorption of [CGR^-] anions was greatly increased by the deprotonation of adsorbents in the pH range of 4–12, due to repulsion towards negatively binding sites of adsorbents by an ion exchange mechanism. The desorption capacity of both adsorbents and the percentage desorption of CGR were calculated from the following equations:

$$q_{\text{desorption}}\left(\text{mg.g}^{-1}\right) = \frac{V \times C_{\text{desorption}}}{\text{Mass}_{\text{adsorbent(g)}}},$$
$$\text{Desorption}(\%)\text{of dyes} = \frac{q_{\text{desorption(mg.g}^{-1})}}{q_{\text{adsorbed(mg.g}^{-1})}} \times 100. \quad (21)$$

4. Conclusion

The peels of watermelon (PWM) and water Chestnuts (PWC) were dried, sieved, and chemically modified with citric acid containing tricarboxylic groups for the adsorption eradication of harmful, venomous, unfriendly, lethal, and tragic, Congo red dyestuffs from the aqueous environment. In this study, the surface orientation of various functional groups and the crystallinity of the peels were evaluated through FT-IR and SEM characterizations. In comparison to the Freundlich statistical data, the Langmuir and Temkin models seem to be more suited for the adsorptive elimination of CGR from aqueous solutions. The correlation coefficients for nonlinear Langmuir, Freundlich, and Temkin isothermal studies are close to unity, 0.99 for adsorptive removal of CGR on each CPWM, PWM, CPWC, and PWC. The q max for nonlinear Langmuir isothermal studies for CPWM and CPWC are 8.3 and 7.95 mg/g, respectively, which are more effective as compared to 2.23 and 4.32 mg/g for their unmodified forms (PWM and PWC), respectively. However, more negative values for Gibbs free energy for acid-modified adsorbents reflect spontaneity, homogeneous, and monolayer adsorption mechanisms. The greater values of BT, 1.4 and 1.3 J/mole, for adsorptive removal of dye on CPWM and CPWC, respectively, as compared to their unmodified forms, PWM and PWC, which are 0.53 and 0.55 J/mole, respectively, indicate the stronger adsorbate-adsorbent associations. The adsorption mechanism follows

pseudo second-order kinetics as the differences between calculated and experimental *qe* (mg/g) are negligible for the adsorptive removal of CGR on CPWM, CPWC, PWM, and PWC, indicating the better fitness of equilibrium data in pseudo second-order kinetics than in first-order mechanism. Moreover, the lowest values for both RMSE and *P* for second-order kinetics support its suitability and acceptability over first-order kinetics. The calculated ΔH^0 for CPWM and CPWC is -145 and -76 kJ/mole, respectively, as compared to PWM and PWC at -57 and -48 kJ/mole, reflecting the stronger adsorbate and adsorbent interactions as well as an exothermic adsorption mechanism. These findings suggest that the CPWM and CPWC adsorbents, which have been treated with citric acid, might be used effectively to remove Congo red dye from wastewater.

Abbreviations

CGR: Congo red dye
PWM: Peels of watermelon
PWC: Peels of water chestnuts
CPWM: Citric acid-treated peels of watermelon
CPWC: Citric acid-treated peels of water chestnuts
pH_{-PZC}: Point of zero charge
FT-IR: Fourier transform-infrared spectroscopy
SEM: Scanning electron microscopy
RMSE: Root mean square errors
P: Percent relative deviation.

Data Availability

All data related to this work is presented in results section along with references.

Conflicts of Interest

We have no conflicts of interest regarding the publication of this paper.

Acknowledgments

We are thankful to COMSAT, Lahore, and LUMS for analysis services.

References

[1] A. Jabeen, X. Huang, and M. Aamir, "The challenges of water pollution, threat to public health, flaws of water laws and policies in Pakistan," *Journal of Water Resource and Protection*, vol. 7, no. 17, pp. 1516–1526, 2015.

[2] I. Sabir, "Water is becoming scarce," *Pakistan Observer*, vol. 28, 2012.

[3] E. M. A. Qureshi, A. U. Khan, and S. Vehra, "An investigation into the prevalence of water borne diseases in relation to microbial estimation of potable water in the community residing near River Ravi, Lahore, Pakistan," *African Journal of Environmental Science and Technology*, vol. 5, no. 8, pp. 595–607, 2011.

[4] R. Sahu, *Removal of Congo Red Dye from Water Using Orange Peel as an Adsorbent, [Ph.D. thesis]*, National Institute of Technology, 2015.

[5] S.-M. Lam, J. C. Sin, A. Z. Abdullah, and A. R. Mohamed, "Degradation of wastewaters containing organic dyes photocatalysed by zinc oxide: a review," *Desalination and Water Treatment*, vol. 41, no. 1-3, pp. 131–169, 2012.

[6] Q. Liu, "Pollution and treatment of dye waste-water," *IOP Conference Series: Earth and Environmental Science*, vol. 514, no. 5, article 052001, 2020.

[7] S. Bhatia and S. Devraj, *Pollution control in textile industry*, WPI Publishing, 2017.

[8] A. Urtiaga, "Electrochemical technologies combined with membrane filtration," *Current Opinion in Electrochemistry*, vol. 27, article 100691, 2021.

[9] R. Bouchareb, Z. Bilici, and N. Dizge, "Water recovery from yarn fabric dyeing wastewater using electrochemical oxidation and membrane processes," *Water Environment Research*, vol. 94, no. 1, article e1681, 2022.

[10] A. V. Filho, R. X. Kulman, N. N. Janner, L. V. Tholozan, A. R. F. de Almeida, and G. S. da Rosa, "Optimization of cationic dye removal using a high surface area-activated carbon from water treatment sludge," *Bulletin of Materials Science*, vol. 44, no. 1, pp. 1–8, 2021.

[11] R. R. Pradhananga, L. Adhikari, R. Shrestha et al., "Wool carpet dye adsorption on nanoporous carbon materials derived from agro-product," *C*, vol. 3, no. 4, p. 12, 2017.

[12] M. Wiafe-Kwagyan, *Comparative bioconversion of rice lignocellulosic waste and its amendments by two oyster mushrooms (Pleurotus species) and the use of the spent mushroom compost as bio-fertilizer for the cultivation of tomato, pepper and cowpea*, University of Ghana, 2014.

[13] R. Reshmy, E. Philip, A. Madhavan et al., "Lignocellulose in future biorefineries: strategies for cost-effective production of biomaterials and bioenergy," *Bioresource Technology*, vol. 344, no. Part B, article 126241, 2022.

[14] S. Dixit and V. L. Yadav, "Green composite film synthesized from agricultural waste for packaging applications," in *Green Composites*, pp. 413–428, Springer, 2021.

[15] M. I. H. Mondal, M. S. Yeasmin, and M. S. Rahman, "Preparation of food grade carboxymethyl cellulose from corn husk agrowaste," *International Journal of Biological Macromolecules*, vol. 79, pp. 144–150, 2015.

[16] A. Abdulrahman, C. Ajani, and S. Aliyu, "Production and characterization of asbestos-free brake lining material using agro wastes," *Engineering and Applied Science Research*, vol. 48, no. 4, pp. 379–384, 2021.

[17] L. Cruz-Lopes, M. Macena, B. Esteves, and I. Santos-Vieira, "Lignocellulosic materials used as biosorbents for the capture of nickel (II) in aqueous solution," *Applied Sciences*, vol. 12, no. 2, p. 933, 2022.

[18] V. Krstić, T. Urošević, M. Uđilanović, A. Ćirić, and S. Milić, "Sorbent based on citrus peel waste for wastewater treatment," in *Nano-Biosorbents for Decontamination of Water, Air, and Soil Pollution*, pp. 455–478, Elsevier, 2022.

[19] D. Gupta, S. M. Mahajani, and A. Garg, "Hydrothermal carbonization of household wet waste - characterization of hydrochar and process wastewater stream," *Bioresource Technology*, vol. 342, article 125972, 2021.

[20] L. H. Velázquez Jiménez, *Adsorption of inorganic priority pollutants in water by tailored lignocellulosic and carbonaceous adsorbents*, Handle Publishing, 2014.

[21] T. V. Tran, D. V. N. Vo, D. T. C. Nguyen, Y. C. Ching, N. T. Nguyen, and Q. T. Nguyen, "Effective mitigation of single-

component and mixed textile dyes from aqueous media using recyclable graphene-based nanocomposite," *Environmental Science and Pollution Research*, vol. 29, no. 21, pp. 32120–32141, 2022.

[22] Z. U. Zango and S. S. Imam, "Evaluation of microcrystalline cellulose from groundnut shell for the removal of crystal violet and methylene blue," *Nanoscience and Nanotechnology*, vol. 8, no. 1, 2018.

[23] M. M. Kabir, M. M. Akter, S. Khandaker et al., "Highly effective agro-waste based functional green adsorbents for toxic chromium(VI) ion removal from wastewater," *Journal of Molecular Liquids*, vol. 347, p. 118327, 2022.

[24] M. de Jesús Nava-Ramírez, A. M. Salazar, M. Sordo et al., "Ability of low contents of biosorbents to bind the food carcinogen aflatoxin B_1*in vitro*," *Food Chemistry*, vol. 345, article 128863, 2021.

[25] M. Sulyman, J. Kucinska-Lipka, M. Sienkiewicz, and A. Gierak, "Development, characterization and evaluation of composite adsorbent for the adsorption of crystal violet from aqueous solution: isotherm, kinetics, and thermodynamic studies," *Arabian Journal of Chemistry*, vol. 14, no. 5, article 103115, 2021.

[26] V. Matko, "Porosity determination by using stochastics method," *Automatika: časopis za automatiku, mjerenje, elektroniku, računarstvo i komunikacije*, vol. 44, no. 3-4, pp. 155–162, 2003.

[27] A. G. A. Joshua and U. P. Ebere, "Kinetics of palm kernel shell in heavy metal ion sorption," *The International Journal of Science and Technoledge*, vol. 3, no. 6, p. 124, 2015.

[28] G. D. Değermenci, N. Değermenci, V. Ayvaoğlu, E. Durmaz, D. Çakır, and E. Akan, "Adsorption of reactive dyes on lignocellulosic waste; characterization, equilibrium, kinetic and thermodynamic studies," *Journal of Cleaner Production*, vol. 225, pp. 1220–1229, 2019.

[29] K. N. Mahmud, T. H. Wen, and Z. A. Zakaria, "Activated carbon and biochar from pineapple waste biomass for the removal of methylene blue," *Environmental and Toxicology Management*, vol. 1, no. 1, pp. 30–36, 2021.

[30] D. Nsubuga, N. Banadda, I. Kabenge, and K. D. Wydra, "Potential of jackfruit waste as anaerobic digestion and slow pyrolysis feedstock," *Journal of Biosystems Engineering*, vol. 46, no. 2, pp. 163–172, 2021.

[31] S. Salem, Z. Teimouri, and A. Salem, "Fabrication of magnetic activated carbon by carbothermal functionalization of agriculture waste via microwave-assisted technique for cationic dye adsorption," *Advanced Powder Technology*, vol. 31, no. 10, pp. 4301–4309, 2020.

[32] B. Magaji, A. U. Maigari, U. A. Abubakar, M. M. Sani, and A. U. Maigari, "Batch adsorption of safranin dye from an aqueous solution of balanites aegyptiaca seed coats," *Asian Journal of Physical and Chemical Sciences*, vol. 8, no. 1, pp. 48–54, 2020.

[33] M. O. Omorogie, M. T. Agbadaola, A. M. Olatunde, B. Helmreich, and J. O. Babalola, "Surface equilibrium and dynamics for the adsorption of anionic dyes onto MnO2/biomass micro-composite," *Green Chemistry Letters and Reviews*, vol. 15, no. 1, pp. 51–60, 2022.

[34] R. J. Martínez, A. Z. Vela-Carrillo, L. A. Godínez, J. D. J. Pérez-Bueno, and I. Robles, "Competitive adsorption of anionic and cationic molecules on three activated carbons derived from agroindustrial waste," Available at SSRN 4053263.

[35] E. Worch, "2 adsorbents and adsorbent characterization," in *Adsorption Technology in Water Treatment*, pp. 14–48, De Gruyter, 2021.

[36] I. Ahmed, Z. Hasan, G. Lee, H. J. Lee, and S. H. Jhung, "Contribution of hydrogen bonding to liquid-phase adsorptive removal of hazardous organics with metal-organic framework-based materials," *Chemical Engineering Journal*, vol. 430, article 132596, 2022.

[37] H. Patel and R. Vashi, "Removal of Congo red dye from its aqueous solution using natural coagulants," *Journal of Saudi Chemical Society*, vol. 16, no. 2, pp. 131–136, 2012.

[38] K. Foo and B. Hameed, "Preparation, characterization and evaluation of adsorptive properties of orange peel based activated carbon via microwave induced K_2CO_3 activation," *Bioresource Technology*, vol. 104, pp. 679–686, 2012.

[39] M. S. Hussain, R. Rehman, and M. Imran, "Comparative evaluation of the adsorption performance of citric acid-treated peels of Trapa natans and Citrullus lanatus for cationic dyes degradation from water," *Journal of Chemistry*, vol. 2022, 19 pages, 2022.

[40] M. S. Hussain, R. Rehman, and M. Imran, "Isothermal and kinetic investigation of exploring the potential of citric acid-treated Trapa natans and Citrullus lanatus peels for Biosorptive removal of brilliant green dye from water," *Journal of Chemistry*, vol. 2021, 23 pages, 2021.

[41] M. Åkerholm, B. Hinterstoisser, and L. Salmén, "Characterization of the crystalline structure of cellulose using static and dynamic FT-IR spectroscopy," *Carbohydrate Research*, vol. 339, no. 3, pp. 569–578, 2004.

[42] P. Sawant and A. S. Dhabe, "FT-IR analysis of in-vivo and in-vitro stem, leaf and callus of Ceropegia bulbosa roxb. var. bulbosa. BIOINFOLET-A quarterly journal of," *Life Sciences*, vol. 19, no. 1, pp. 46–50, 2022.

[43] Y. Zhao, C. Xing, C. Shao et al., "Impacts of intrinsic alkali and alkaline earth metals on chemical structure of low-rank coal char: semi-quantitative results based on FT-IR structure parameters," *Fuel*, vol. 278, article 118229, 2020.

[44] O. Yılmaz and N. Tugrul, "Zinc adsorption from aqueous solution using lemon, orange, watermelon, melon, pineapple, and banana rinds," *Water Practice & Technology*, vol. 17, no. 1, pp. 318–328, 2022.

[45] A. S. El-Shafie, S. S. Hassan, N. Akther, and M. El-Azazy, "Watermelon rinds as cost-efficient adsorbent for acridine orange: a response surface methodological approach," *Environmental Science and Pollution Research*, pp. 1–20, 2021.

[46] F. Falope, A. Akinlabi, and M. Idowu, "Assessment of physico-mechanical properties of natural rubber and modified natural rubber vulcanizates with watermelon rind as fillers," *Journal of Applied Sciences and Environmental Management*, vol. 26, no. 5, pp. 823–828, 2022.

[47] Y. Guan, M. Xia, X. Wang, W. Cao, and A. Marchetti, "Water-based preparation of nano-sized NH_2-MIL-53(Al) frameworks for enhanced dye removal," *Inorganica Chimica Acta*, vol. 484, pp. 180–184, 2019.

[48] D. Zewde and B. Geremew, "Removal of Congo red using Vernonia amygdalinaleaf powder: optimization, isotherms, kinetics, and thermodynamics studies," *Environmental Pollutants and Bioavailability*, vol. 34, no. 1, pp. 88–101, 2022.

[49] S. Chatterjee, N. Guha, S. Krishnan, A. K. Singh, P. Mathur, and D. K. Rai, "Selective and recyclable Congo red dye adsorption by spherical Fe3O4 nanoparticles functionalized with 1, 2,

4, 5-benzenetetracarboxylic acid," *Scientific Reports*, vol. 10, no. 1, pp. 1–11, 2020.

[50] E. Demirbas, N. Dizge, M. T. Sulak, and M. Kobya, "Adsorption kinetics and equilibrium of copper from aqueous solutions using hazelnut shell activated carbon," *Chemical Engineering Journal*, vol. 148, no. 2-3, pp. 480–487, 2009.

[51] M. A. Darweesh, M. Y. Elgendy, M. I. Ayad, A. M. M. Ahmed, N. M. K. Elsayed, and W. A. Hammad, "Adsorption isotherm, kinetic, and optimization studies for copper (II) removal from aqueous solutions by banana leaves and derived activated carbon," *Chemical Engineering*, vol. 40, pp. 10–20, 2022.

[52] D. Sachdev, H. Shrivastava, S. Sharma et al., "Potential for hydrothermally separated groundnut shell fibers for removal of methylene blue dye," *Materials Today: Proceedings*, vol. 48, pp. 1559–1568, 2022.

[53] S. Bachmann, I. V. J. Dávila, T. Calvete, and L. A. Féris, "Adsorption of Cr (VI) on lignocellulosic wastes adsorbents: an overview and further perspective," *International journal of Environmental Science and Technology*, pp. 1–22, 2022.

[54] P. K. Malik, "Use of activated carbons prepared from sawdust and rice-husk for adsorption of acid dyes: a case study of acid yellow 36," *Dyes and Pigments*, vol. 56, no. 3, pp. 239–249, 2003.

[55] Z. Isik, M. Saleh, I. M'barek, E. Yabalak, N. Dizge, and B. Deepanraj, "Investigation of the adsorption performance of cationic and anionic dyes using hydrochared waste human hair," *Biomass Conversion and Biorefinery*, pp. 1–14, 2022.

[56] N. U. M. Nizam, M. M. Hanafiah, E. Mahmoudi, A. W. Mohammad, and A. A. Oyekanmi, "Effective adsorptive removal of dyes and heavy metal using graphene oxide based pre-treated with NaOH / H_2SO_4 rubber seed shells synthetic graphite precursor: equilibrium isotherm, kinetics and thermodynamic studies," *Separation and Purification Technology*, vol. 289, article 120730, 2022.

[57] M. A. Rahaman, M. T. H. Sumon, S. Razia, and M. A. Rashed, "A comparative study of the adsorptive removal of toxic amaranth dye from aqueous solution using low cost bio-adsorbents," *IJCS*, vol. 10, no. 1, pp. 106–113, 2022.

[58] C. H. Bolster and G. M. Hornberger, "On the use of linearized Langmuir equations," *Soil Science Society of America Journal*, vol. 71, no. 6, pp. 1796–1806, 2007.

[59] A. Tehrim, M. Dai, X. Wu et al., "Citric acid modified waste cigarette filters for adsorptive removal of methylene blue dye from aqueous solution," *Journal of Applied Polymer Science*, vol. 138, no. 27, p. 50655, 2021.

[60] U. Kamran, H. N. Bhatti, S. Noreen, M. A. Tahir, and S. J. Park, "Chemically modified sugarcane bagasse-based biocomposites for efficient removal of acid red 1 dye: kinetics, isotherms, thermodynamics, and desorption studies," *Chemosphere*, vol. 291, article 132796, 2022.

[61] M. A. Kadhum, A. J. Kadhim, and A. M. Aljeboree, "Enhanced removal of phenylephrine hydrochloride using eco-friendly surface: optimization, isotherm, kinetics, and regeneration studies," *Quality Assurance*, vol. 12, no. 3, pp. 206–210, 2021.

[62] A. S. Al-Wasidi, I. I. AlZahrani, H. I. Thawibaraka, A. M. Naglah, M. G. El-Desouky, and M. A. El-Bindary, "Adsorption studies of carbon dioxide and anionic dye on green adsorbent," *Journal of Molecular Structure*, vol. 1250, article 131736, 2022.

[63] A. Alagarsamy, S. Chandrasekaran, and A. Manikandan, "Green synthesis and characterization studies of biogenic zirconium oxide (ZrO_2) nanoparticles for adsorptive removal of methylene blue dye," *Journal of Molecular Structure*, vol. 1247, article 131275, 2022.

[64] F. Hamidi, M. H. Dehghani, M. Kasraee, M. Salari, L. Shiri, and A. H. Mahvi, "Acid red 18 removal from aqueous solution by nanocrystalline granular ferric hydroxide (GFH); optimization by response surface methodology & genetic- algorithm," *Scientific Reports*, vol. 12, no. 1, pp. 1–15, 2022.

[65] H. Chandarana, P. Senthil Kumar, M. Seenuvasan, and M. Anil Kumar, "Kinetics, equilibrium and thermodynamic investigations of methylene blue dye removal using *Casuarina equisetifolia* pines," *Chemosphere*, vol. 285, article 131480, 2021.

[66] H.-J. Choi, "Assessment of sulfonation in lignocellulosic derived material for adsorption of methylene blue," *Environmental Engineering Research*, vol. 27, no. 3, 2022.

[67] S. Salvestrini, L. Ambrosone, and F.-D. Kopinke, "Some mistakes and misinterpretations in the analysis of thermodynamic adsorption data," *Journal of Molecular Liquids*, vol. 352, article 118762, 2022.

[68] R. Zein, L. Hevira, Zilfa, Rahmayeni, S. Fauzia, and J. O. Ighalo, "The improvement of indigo carmine dye adsorption by Terminalia catappa shell modified with broiler egg white," *Biomass Conversion and Biorefinery*, pp. 1–18, 2022.

[69] F. Alakhras, H. Ouachtak, E. Alhajri et al., "Adsorptive removal of cationic rhodamine B dye from aqueous solutions using chitosan-derived schiff base," *Separation Science and Technology*, vol. 57, no. 4, pp. 542–554, 2022.

[70] K. Oukebdane, I. L. Necer, and M. Didi, "Binary comparative study adsorption of anionic and cationic azo-dyes on Fe3O4-bentonite magnetic nanocomposite: kinetics, equilibrium, mechanism and thermodynamic study," *SILICON*, pp. 1–14, 2022.

[71] N. Harisah, D. Siswanta, M. Mudasir, and S. Suyanta, "Superparamagnetic composite of magnetite-CTAB as an efficient adsorbent for methyl orange," *Indonesian Journal of Chemistry*, vol. 22, no. 2, pp. 387–401, 2022.

[72] S. J. Britto, E. Amutha, E. Pushpalaksmi et al., "Linear and non-linear regression analysis for the sorption kinetics of rhodamine dye from aqueous solution using chitosan-jackfruit nanocomposite," *Journal of Applied Sciences and Environmental Management*, vol. 26, no. 1, pp. 91–104, 2022.

[73] T. S. Munonde, N. P. September, A. Mpupa, and P. N. Nomngongo, "Two agitation routes for the adsorption of reactive red 120 dye on NiFe LDH/AC nanosheets from wastewater and river water," *Applied Clay Science*, vol. 219, article 106438, 2022.

[74] A.-D. Mai and P. B. Pathare, "Kinetic modeling of quality changes of tomato during storage," *Agricultural Engineering International: CIGR Journal*, vol. 23, no. 1, pp. 183–193, 2021.

[75] A. G. Tarone, E. K. Silva, C. B. Betim Cazarin, and M. R. Marostica Junior, "Inulin/fructooligosaccharides/pectin-based structured systems: promising encapsulating matrices of polyphenols recovered from jabuticaba peel," *Food Hydrocolloids*, vol. 111, article 106387, 2021.

[76] R. Ghibate, O. Senhaji, and R. Taouil, "Kinetic and thermodynamic approaches on rhodamine B adsorption onto pomegranate peel," *Case Studies in Chemical and Environmental Engineering*, vol. 3, article 100078, 2021.

[77] P. Vairavel, N. Rampal, and G. Jeppu, "Adsorption of toxic Congo red dye from aqueous solution using untreated coffee husks: kinetics, equilibrium, thermodynamics and desorption

study," *International Journal of Environmental Analytical Chemistry*, pp. 1–20, 2021.

[78] P. Saha, S. Chowdhury, S. Gupta, and I. Kumar, "Insight into adsorption equilibrium, kinetics and thermodynamics of malachite green onto clayey soil of Indian origin," *Chemical Engineering Journal*, vol. 165, no. 3, pp. 874–882, 2010.

[79] Z. R. Zair, Z. T. Alismaeel, M. Y. Eyssa, and M. J. M-Ridha, "Optimization, equilibrium, kinetics and thermodynamic study of Congo red dye adsorption from aqueous solutions using iraqi porcelanite rocks," *Heat and Mass Transfer*, vol. 58, no. 8, pp. 1393–1410, 2022.

[80] R. Ahmed, R. R. Rafia, and M. A. Hossain, "Kinetics and thermodynamics of acid red 1 adsorption on used black tea leaves from aqueous solution," *International Journal of Sciences*, vol. 10, no. 6, pp. 7–15, 2021.

[81] C. A. Igwegbe, O. D. Onukwuli, J. O. Ighalo, and P. U. Okoye, "Adsorption of cationic dyes on Dacryodes edulis seeds activated carbon modified using phosphoric acid and sodium chloride," *Environmental Processes*, vol. 7, no. 4, pp. 1151–1171, 2020.

[82] K. Gul, S. Sohni, I. Ahmad et al., "Synthesis and characterization of graphene/Fe3O4 nanocomposite as an effective adsorbent for removal of acid red-17 and remazol brilliant blue R from aqueous solutions," *Current Nanoscience*, vol. 12, no. 5, pp. 554–563, 2016.

[83] I. Ghaeli, *Developing Antimicrobial Collagen/Silk Fibroin Biocomposites with Immobilized Phages*, Faculty of Engineering of the University of Porto, 2018.

[84] M. E. Mahmoud, S. M. Elsayed, S. E. M. Mahmoud, R. O. Aljedaani, and M. A. Salam, "Recent advances in adsorptive removal and catalytic reduction of hexavalent chromium by metal-organic frameworks composites," *Journal of Molecular Liquids*, vol. 347, no. article 118274, 2021.

[85] F. G. M. Borsagli, "A Green 3D Scaffolds Based on Chitosan with Thiol Group as a Model for Adsorption of Hazardous Organic Dye Pollutants," *Carbon*, vol. 4, no. 7, pp. 12-13, 2019.

[86] F. Amran and M. A. A. Zaini, "Sodium hydroxide-activated *Casuarina* empty fruit: Isotherm, kinetics and thermodynamics of methylene blue and congo red adsorption," *Environmental Technology & Innovation*, vol. 23, article 101727, 2021.

[87] J.-W. Lee and T. W. Jeffries, "Efficiencies of acid catalysts in the hydrolysis of lignocellulosic biomass over a range of combined severity factors," *Bioresource Technology*, vol. 102, no. 10, pp. 5884–5890, 2011.

[88] T. A. Khan, S. Sharma, E. A. Khan, and A. A. Mukhlif, "Removal of Congo red and basic violet 1 by chir pine (Pinus roxburghii) sawdust, a saw mill waste: batch and column studies," *Toxicological & Environmental Chemistry*, vol. 96, no. 4, pp. 555–568, 2014.

[89] R. Rehman, I. Manzoor, and L. Mitu, "Isothermal study of Congo red dye biosorptive removal from water by Solanum tuberosum and Pisum sativum peels in economical way," *Bulletin of the Chemical Society of Ethiopia*, vol. 32, no. 2, pp. 213–223, 2018.

[90] M. Stjepanović, N. Velić, A. Galić, I. Kosović, T. Jakovljević, and M. Habuda-Stanić, "From waste to biosorbent: removal of Congo red from water by waste wood biomass," *Water*, vol. 13, no. 3, p. 279, 2021.

[91] B. G. Alhogbi, S. Altayeb, E. A. Bahaidarah, and M. F. Zawrah, "Removal of anionic and cationic dyes from wastewater using activated carbon from palm tree fiber waste," *PRO*, vol. 9, no. 3, p. 416, 2021.

[92] A. Extross, A. Waknis, C. Tagad, V. V. Gedam, and P. D. Pathak, "Adsorption of Congo red using carbon from leaves and stem of water hyacinth: equilibrium, kinetics, thermodynamic studies," *International journal of Environmental Science and Technology*, pp. 1–38, 2022.

[93] D. Rady, M. Shaban, K. N. M. Elsayed et al., "Experimentally and theoretically approaches for Congo red dye adsorption on novel kaolinite-alga nano-composite," *International Journal of Environmental Analytical Chemistry*, pp. 1–23, 2021.

[94] W. C. Wanyonyi, J. M. Onyari, and P. M. Shiundu, "Adsorption of Congo red dye from aqueous solutions using roots of Eichhornia crassipes: kinetic and equilibrium studies," *Energy Procedia*, vol. 50, pp. 862–869, 2014.